Fall 2017

Nanoparticles: nanoscale systems for medical applications

David Allen Wadkins
University of Iowa

NANOPARTICLES:
NANOSCALE SYSTEMS FOR MEDICAL APPLICATIONS

by

David Allen Wadkins

A thesis submitted in partial fulfillment
of the requirements for the Master of Science
degree in Biomedical Engineering in the
Graduate College of
The University of Iowa

December 2017

Thesis Supervisor: Assistant Professor James A. Ankrum

Graduate College
The University of Iowa
Iowa City, Iowa

CERTIFICATE OF APPROVAL

_____

MASTER'S THESIS

_____

This is to certify that the Master's thesis of

David Allen Wadkins

has been approved by the Examining Committee for
the thesis requirement for the Master of Science degree
in Biomedical Engineering at the December 2017 graduation.

Thesis Committee: _____
James A. Ankrum, Thesis Supervisor

_____
Aliasager Salem

_____
Edward Sander

ACKNOWLEDGEMENTS

I owe a great debt of gratitude to my PI and advisor Dr. James Ankrum for the incredible amount of support that he provided me during the course of this thesis work. Few people that I have encountered in my 25 years have the same level of caring, knowledge and dedication that he has, and There are fewer words that can convey my appreciation for the atmosphere that Dr. Ankrum fosters in his lab. His passion for educating helped inspire me to find my own passion, and his guidance has been fundamental in my education as an engineer and young scientist. I will forever be grateful to Dr. Ankrum and firmly believe that I would have been hard pressed to find a better mentor at the University of Iowa. I wish him the best of luck in all aspects of his life.

In addition to my mentor, I would like to express my appreciation to the remainder of my thesis committee: Dr. Aliasager Salem, and Dr. Edward Sander. Both are phenomenal professors who taught challenging, yet fair and engaging classes that helped deepen my understanding of the sciences. I would also like to thank them for their critical feedback and insight that helped me to focus and refine this thesis.

I would also like to express my gratitude to Dr. Matthew Potthoff, Dr. Al Klingelhultz, Dr. Katie Markan, and Dr. Brandon Davies, who collaborated on my projects and helped to facilitate experiments that were critical to this thesis.

To my fellow Graduate students in the Ankrum Lab; Tony Burand, Lauren Boland, Alex Brown, and Michael Schrodt, thank you for making the lab enjoyable, and inspiring me with your incredible work ethic, and knowledge. You have all been invaluable in providing feedback, proofreading, and scientific insight for all my projects.

Finally, to my Family, simply put, I love you and could not have done this without you.

ABSTRACT

The goal of this project was to develop a series of nano platforms for single cell analysis and drug delivery. Nanoparticles are a promising option to improve our medical therapies by controlling biodistribution and pharmacokinetics of therapeutics. Nanosystems also offer significant opportunity to improve current imaging modalities. The systems developed during this thesis work can be foundations for developing advanced therapies for obesity and improving our fundamental understandings of single cell behavior.

The first of the two systems we attempt to create was a drug delivery system that could selectively target adipose tissue to deliver uncoupling agents and drive browning of adipose tissue and associated weight loss. Protonophores have a history of significant toxic side effects in cardiac and neuronal tissues a recently discovered protonophore, but BAM-15, has been shown to have reduced cytotoxicity. We hypothesized that the altered biodistribution of BAM-15 encapsulated in a nanoparticle could provide systemic weight loss with minimized side effects.

The second system developed utilized quantum dots to create a fluorescent barcode that could be repeatedly identified using quantitative fluorescent emission readings. This platform would allow for the tracking of individual cells, allowing repeat interrogation across time and space in complex multicellular environments.

Ultimately this work demonstrates the process and complexity involved in developing nanoparticulate systems meant to interact with incredibly complex intracellular environments.

PUBLIC ABSTRACT

Nanoparticles are extremely promising tools that we can use to better understand the behavior of cells and improve the quality of our medical therapies. They can be used as tools to study how our cells and bodies react to certain stimuli improving our fundamental knowledge of nature. Or they can be used to deliver drugs in more effective, safer, and often cheaper ways. Unfortunately, for each of these applications, it takes considerable work to optimize and characterize the interactions between these particles, the payload they contain and living cells. This thesis reviews the basic underlying properties of nanoparticles, the materials they are made from, and the processes used to develop these systems.

By developing these technologies, we hope to create tools that doctors and other scientists can use to improve their treatments and research. My work demonstrates how to develop these technologies at an early stage and looks at the complex interactions that occur when these systems are introduced to living cells.

TABLE OF CONTENTS

LIST OF TABLES

LIST OF FIGURES

CHAPTER 1: INTRODUCTION

Many materials have been formulated into systems on a nanometer scale that have unique and promising new properties, these systems are often referred to as nanoparticles and can be used for a wide range of biomedical applications. Imaging and pharmaceutical nanoparticles are traditionally polymeric or metallic particles ranging in size from one to a few thousand nanometers, and can be utilized for everything from drug delivery to being contrast agents for various imaging techniques. Though the term nanoparticle is technically described as being a particle with at least one dimension less than 100 nm, it is common in the field to refer to particles up to the micron size as nanoparticles. Particles in the range of 100-1000 nm can more accurately be described as sub-micron particles with larger particles being correctly termed microparticles. However, for the sake of simplicity, I will be referring to most of the particulate systems in this thesis as nanoparticles despite them primarily existing in the sub-micron regime.

Such systems are primarily stored either: dispersed in a liquid suspension for easy administration or processed into dry powders that can allow for either pulmonary delivery, extended storage or further processing into other delivery formulations. One of the major concerns with nanoparticle design is ensuring that they be biocompatible and biodegradable. These features as well as the release and degradation profiles are largely a product of the material chosen for the nanoparticle. To this end materials commonly used are proteins, macromolecules such as lipids and commonly synthetic polymers. These materials can easily be formulated into a variety of nano and micro sized systems through a number of well characterized methods such as: flow focusing, single emulsion systems for hydrophobic agents, double emulsion systems for hydrophilic agents, Spray drying and nanoprecipitation.

During the decades of research into nanoparticle systems, several of them have made their way through clinical trials, one product, Abraxane, is a 130 nm albumin bound paclitaxel delivery system. Other cancer therapeutic agents are currently being tested in nanoparticle systems but much

work still needs to be done on these systems to ensure reproducibility for commercial scale production as well as extreme control over the delivery kinetics. Cancer therapeutics are some of the most commonly studied for these delivery systems as nanoparticles offer extreme promise in the reduction of toxic side effects and increased efficacy. However, these are not the only molecules encapsulated in nanoparticles. Other common therapeutics are genes, proteins, peptides and other macromolecules that are readily inactivated in the body via various mechanisms. The nanoparticle systems help to maintain the bioactivity of the biologics as well as helping to provide improved delivery targeting.

Traditionally many nanoparticles and other systemically administered drugs are sequestered by macrophages causing localization of particles primarily to the liver, spleen and other off target locations. However, functionalization of nanoparticle surfaces with poly-ethylene glycol or other similar extremely hydrophilic polymers can result in "stealth" nanoparticles that are able to avoid the bodies clearance mechanisms enabling increased half-life of the nanoparticles in systemic circulation. Other forms of surface modification can result in improved targeting, responsiveness to changing environments, or even delivery across previously difficult to permeabilize barriers such as the blood brain barrier.

While much of the research currently being done on nanoparticle systems is focused on drug delivery they offer excellent promise as contrast agents for various imaging technologies ranging from ramen spectroscopy to single cell tracking and imaging. Unfortunately, many of the nanoparticles designed to provide improvements in imaging techniques require non-biodegradable components such as iron-oxide, or other metals. This creates difficulties as the nanoparticulate systems reach market and as they transition to human use from animal models. When transitioning to larger more complex organisms concerns about toxicology, and toxicity of degradation products becomes increasingly important. For this reason, many nanoparticulate systems utilize well

characterized polymer systems such as the copolymers of poly lactic acid and poly glycolic acid, frequently referred to together as poly lactic co glycolic acid or PLGA.

For the purposes of this thesis, many of the nanoparticle systems have gone through a number of formulation phases in which different materials were used, however many of them ended up utilizing PLGA as the primary polymer, created through widely used single emulsion methods. These nanoparticle systems than underwent further surface functionalization through layer by layer coating or common NHS-EDC, and biotinylating reactions. This thesis will focus on the process engineering used to optimize the production and encapsulation of drug delivery nanoparticles, the functionalization of their surface for improved bioavailability and targeting. Following this I will shift my focus to the process of developing a novel single cell tracking system, and the unexpected complications arising from the complexity of the intracellular environment.

CHAPTER 2: LITERATURE REVIEW

2. Preface

Nanoparticles have a wide range of applications in the biomedical sciences. In this chapter many aspects of nanoparticle formulation and design will be discussed, starting with the unique properties that make nanoparticles so promising for pharmaceutical drug delivery applications. Following this, nanoparticles utilized for gene therapy and vaccine delivery will be addressed. Before moving on to nanoparticles designed to interrogate the behavior of cells and improve our imaging modalities. Finally, the fundamental physical properties that define nanoparticles and the materials that help produce these unique properties will be analyzed.

2.1. Medical Applications

2.1.1. Drug Delivery

Perhaps the most impactful use of nanoparticle systems is their potential to be used for a variety of medical applications. Especially notable among these applications is their use as drug delivery systems (DDS). Nanoparticles make extremely promising avenues for the delivery of therapeutics due to their ability to enhance or provide controlled release of drugs[1,2], active and inactive targeting[3–6], and potential alleviation of toxic side effects of therapeutics[7]. Due to their size, nanoparticle systems allow for a different profile of bioavailability and pharmacokinetics than is characteristic of the drug load they may be delivering, allowing an additional parameter by which to tune focused and optimal drug delivery to specific tissue beds.

The most critical of these benefits is the ability of nanoparticles to both actively and inactively target specific tissues for the delivery of biologic agents. Early mechanisms of targeting exploited the passive accumulation of nanoparticles in various tissues such as lymph nodes, the spleen and tumor lesions[8,9]. Perhaps the most iconic example of this was the leveraging of the enhanced permeability and retention (EPR) aspect of tumors. The EPR feature of the tumors

microenvironment (TME) is a byproduct of the increased vascularization of the tumor[10]. Tumors often exhibit elevated levels of vascular endothelial growth factor (VEGF), and other cytokines that collectively drive an extremely rapid expansion of tumor vasculature[11]. The elevated rate of vascular expansion in the within the TME leads to vasculature that is often not well formed and therefore "leaky". This increased permeability of the vasculature in the microenvironment allows the nanoparticles to easily exit the vasculature and accumulate in the interstitial space of the tumor[6,12,13]. Further, the leakiness of the tumor vasculature produces an increase in hydrostatic pressure in the interstitial spaces helping to retain particles in these locations. This results in a gradual buildup of nanoparticles in the tumor.[6]

Unfortunately, the EPR effect of the TME is widely regarded as being an insufficient targeting method by itself[14]. It is often considered insufficient because nanoparticles are still cleared from systemic circulation by the kidney, spleen and liver filtration processes. As these organs filter nanoparticles, nanoparticle accumulation can also occur within these tissue beds[15,16]. Additionally, depending on the size of the nanoparticle system, it is not uncommon to see particle accumulation in the capillary beds of the lungs or within the lymph nodes.[8,15] Accumulation in these areas ultimately limits the amount that reaches and stays in the target environment. Loss of nanoparticles to these and other tissues means that a tumor, regardless of size typically will only see between 1 and 10% of the total dose.[17] Unfortunately, because this is an issue of insufficient on-target delivery, simple fixes like increasing dose cannot be pursued because the accumulation in off-target tissue beds would likely lead to more severe side effects.

A key step in developing truly targeted nanoparticles was to design a mechanism to reduce clearance by the filtration and immune systems of the body. Conjugation of polyethylene glycol, or other hydrophilic polymers, to the surface of nanoparticles, is an extremely prevalent mechanism for improving the efficiency of drug delivery from nanoparticles[18–20]. PEGylation, the process of conjugating polyethylene glycol to a nanosystem, is one of the most popular methods of achieving

this as it is a biocompatible polymer that has demonstrated significant improvements in DDS efficiency. PEG functions by creating a brush of extremely hydrophilic polymers around the nanoparticle, which likely creates a corona of water molecules that move into regions surrounding the PEG groups[20]. The corona-like integration of water molecules leads to several desirable outcomes including reduced nanoparticle aggregation, as well as decreased interaction with many serum and tissue proteins. It is this effect that results in its "stealth" behavior, and PEG has been shown to reduce uptake by the reticuloendothelial system (RES) and increase circulation time[21]. These improvement have even been shown to reduce accumulation of PEGylated particles in the liver by as much as 50% - 66%[22] when compared to non-PEGylated nanoparticles of the same size. Other mechanisms exist to improve circulation half-life and will be discussed further in chapter 2.5.2 along with additional discussion on PEG.

Once PEGylation was shown to enhance passive targeting strategies by increasing circulation time and promoting greater nanoparticle accumulation within the TME,[22] attention in the field was then redirected to the development of truly targeted nanoparticles via incorporation of active targeting systems. Active targeting systems typically involve the incorporation of functional groups that have strong binding affinities to cellular components to the exterior of a nanoparticle. It is becoming increasingly common to bind targeting moieties, such as anti-bodies or other peptides, to the shell of nanoparticles[23–25]. These anti-bodies or proteins are chosen due to their high degree of specificity to a target tissue antigen as well as strong binding affinity to proteins expressed on the surfaces of the desired cell lines. Through optimized protein design and enhanced discovery of highly tissue-specific antigenic targets, improvements have been possible in driving preferential accumulation in target tissues[26–28].

By creating a nanoparticle that preferentially accumulates in a target organ or tissue of choice it is possible to reduce the dose of free drug with which the rest of the body interacts[18]. For the delivery of chemotherapeutics, which have narrow therapeutic windows, and therefore a high

likelihood of toxic off-target side effects, the potential benefits of targeting become significant. By reducing the dose of drug reaching off-target sites, through either passive accumulation in the TME, increased circulation time via PEGylation, or pursuing active targeting strategies, both the probability and severity of chemotherapeutic side effects can be diminished[7,29,30]. Several nanosystem formulations incorporating chemotherapeutic drugs are already commercially available and have demonstrated decreased incidence of side effects[12], which has prompted increased interest in further research and optimization. As additional research is generated to optimize the specificity of targeting methods, the range of tissue targets and strength of the decreased side effect profile will only expand. As previously mentioned, work by Chan et al. demonstrated only 10% or less of a dose reaches a particular tissue; however, by improving the percent of particles localizing to the target tissues, lower initial doses of drug could be utilized with the aim of decreasing toxic side effects and enhancing quality of life for patients undergoing chemotherapy

Another promising area of research aiming to decrease off-target drug effects is the use of controlled drug release from nanoparticle systems[31,32]. Drugs have an inherent therapeutic window[33], which is the range of concentrations in which the drug demonstrates the desired therapeutic effect with little or no toxic side effects. Unfortunately, many drugs, especially chemotherapeutics, have narrow therapeutic windows[33,34]. When drugs have a narrow therapeutic window, optimal dosing can be difficult to achieve; too conservative of a dose means not achieving optimal therapeutic effect, while too high of a dose means increased toxic effects. The ideal drug delivery system would be one that includes the ability to rapidly introduce enough drug to be within the therapeutic window followed by a sustained release of drug at the same rate the body metabolizes said drug. In addition to slowly releasing drug to maintain drug concentrations at required levels, having a system that can maintain delivery for days or weeks at a time can be highly desirable in chronic indications like: pain management, antibiotic delivery, or

chemotherapy regiments. However, this is a property that would be relatively unnecessary in the treatment of minor and acute indications like nausea.

Poly Lactic-co-Glycolic Acid (PLGA) nanoparticles are particularly well known for long-term sustained release[1]**.** Degradation kinetics for PLGA nanoparticles can range from a few days to a month depending on the molecular weight, and inherent viscosity of the PLGA[2]. Acetalated dextran, another polymer used for nanoparticle formation, has degradation kinetics that can be modified such that it degrades within either 16 +/- 10 min to as much as 27 +/- 1 hour[35]. by controlling the ratio of cyclic to acyclic acetals. Drug release kinetics and degradation properties of materials are driven by complex interactions between a number of physical properties including, but not limited to: polymer molecular weight, chain length, viscosity, morphology, drug polymer interactions, drug molecular weight, solubility, loading density, release environment and chemical composition[36]. A sustained release profile, in addition to making drug delivery potentially more effective and safer, can generate additional benefits for the patient. By creating delivery systems that gradually release drugs, the number of times that the drug needs to be administered could be reduced. Decreasing the number of drug administrations could help resolve issues with patient compliance, comfort, lifetime dosing issues associated with drugs like doxorubicin[37–39], and drug concentration variability[36].

While controlling the release rate of a drug is desirable to maintain drug concentration in its therapeutic window, this strategy still carries risk of drug exposure to the entire body. Further maintaining concentration at a therapeutic window can be exceptionally challenging depending on the drug and the individual's metabolism. To overcome these limitations and further improve controlled drug release, it is possible to develop environmentally responsive nanoparticles, which only release the encapsulated drug payload after activation by a secondary stimulus. There are several approaches already being explored to improve selective drug release, among these strategies is the development of a hydrogel that is extremely stable until exposed to therapeutic ultrasound,

the excitation of the ultrasound causes cavitation in the hydrogel and breaks it apart[31,40,41]. Once the particle has been broken it releases its encapsulated drug to the local area. Unfortunately, this approach does not prevent the released drug from then spreading, and as such more work is needed to control the rate of degradation following application of the ultrasound stimulus. This system is currently being studied for the delivery of BMP therapeutics to promote bone healing and has shown promise[31]. They demonstrated almost complete selectivity of release following stimulation with ultrasound. Similar hydrogels and polymers have been developed that are temperature[42–44], pH[45–48] or light responsive[49–51].

Ritter et al. largely pioneered the development of thermo-responsive hydrogel systems by incorporating N-isopropylacrylamide monomers[52]. Thermoresponsive polymers are typically chains that exist in a coil like conformation that will compact or expand depending on temperature. The heat range in which this occurs is referred to as the upper and lower critical solution temperatures[42–44]. Unfortunately, it can often be challenging to control temperature or photo-enervation in-vivo so pH responsive polymers tend to be a bit more popular.

PH responsive polymers are extremely popular strategies as there are several niches *in-vivo* that have specific pH properties. Perhaps most significant of these is the fact that tumors typically possess acidic micro-environments, an aspect that is often targeted by these systems. pH responsive polymers have also been exploited for gastrointestinal delivery, and to escape lysosomal niches for cytoplasmic delivery of therapeutics[53]. Poly (methacrylic acid) based particles (PMAA-NP) are widely explored for the delivery of fragile peptides like insulin. PMAA-NP remain collapsed and hydrophobic through the acidic environment of the stomach and expand when carboxyl groups lose protons in the gastric passages alkaline pH. This strategy allows for safe passage of peptides like insulin through the stomach to the intestines where it can be absorbed[54,55]. Continued advances in this technology could soon provide oral insulin therapies for diabetic populations, a significant improvement in delivery strategy. Tumors are another widely exploited target due to them

exhibiting pH states that can be as low as 5.7[56]. Griset et al. demonstrated hydrogels that swelled in response to the acidic pH of tumors by cross linking hydrophobic acrylic based polymers with hydroxyl groups. The hydroxyl groups were protected by 2,4,6-trimethoxybenzaldehyde, a pH labile moiety. These particles were shown to be stable in neutral environments, and even mildly acidic environments could cleave the protecting groups. Following cleavage, the particle transitions from hydrophobic to hydrophilic driving swelling of the gel and release of encapsulated therapeutics[53,57].

2.1.2. Gene Delivery

Gene therapy is a growing area of research, and the delivery of genetic materials is a promising therapeutic strategy for many indications. This therapeutic approach utilizes protein encoding genes to modify endogenous genes to correct disease states from heart failure to cancer[58–60]. Considering the potential of this therapeutic strategy it becomes critical to find an efficient delivery method for DNA and other genetic materials. Although naked DNA can be delivered for gene therapies this approach is very inefficient due to the negative charge in both the DNA molecules and the cellular membrane cause repulsion instead of association. Further naked genetic materials can be detected by TLRs leading to undesirable side effects. Therefore, it becomes necessary to utilize vectors to improve the delivery of genetic material.[61,62] There are two main types of vectors currently being utilized to improve the efficiency of genetic material uptake: viral and non-viral[63]. Non-viral carriers like nanoparticles, are typically simple to prepare, can be readily modified and are less immunogenic[62]. While on the other hand viral vectors are typically more efficient than non-viral vectors. However, viral vectors present significantly more risk and can be highly immunogenic[64,65] with several children famously passing away during a clinical trial as the result of these dangers[66].

The safety concerns associated with viral modification such as insertion mutagenesis, or the risk of extreme immune responses such as a cytokine storm makes non-viral vectors' safety

particularly appealing. Advances in nanotechnology have enabled it to become a significant part in the development of novel, efficient non-viral vectors[63]. In addition to protecting the organism from the dangers of the genetic material or a viral vector such as cytokine storms or immune recognition, nanoparticles can also protect: hydrophobic peptides[67], siRNA[68,69], DNA molecules[60,70], and other genetic materials from the hostile environment *in-vivo*. Despite the promise these materials have they face a number of hurdles in the form of enzymatic degradation, the innate and adaptive immune system, and rapid renal excretion[71,72]. Fortunately, several groups have developed cationic lipid or polymer Nano systems to improve their cytosolic delivery, and protect them from serum nucleases and MPS recognition[73–76]. Similar success have been seen with plasmid DNA[77] as well as peptide and other proteins[78,79]. The ability of nanoparticles to protect hydrophobic small molecules from the host opens the possibility of them being used as adjuvants and delivery mechanisms for vaccines and immunotherapies which often utilize these types of molecules.

2.1.3. Vaccine Delivery

New generations of vaccines are increasingly oriented towards minimalist designs that decrease the immunogenicity of the treatment[80]. This in turn makes formulations that modulate the effectiveness of vaccines increasingly important to compensate for the decreased immunogenicity. Nanoparticles, when formulated optimally, can improve antigen immunogenicity and stability while also benefiting from the previously discussed ability of nanoparticles to target specific tissues, as well as their sustained release profiles[80]. In fact, a number of therapeutic and prophylactic vaccine delivery systems have already been FDA aproved[70], for everything from hepatitis A[83] to influenza[84] with more prophylactic systems in clinical trials[85,86]. Part of the reason that nanoparticles make such promising vaccine carriers is the fact that many polysaccharide base polymers such as alginate[87], acetalated dextran[88], chitosan[89], and pullulan[90,91] have all exhibited adjuvant properties *in-vitro*. Acetalated dextran in particular has shown significant increases in antigen presentation by both MHC I and MHC II[88] *in-vitro*. In addition to polymeric systems, several inorganic

formulations have been developed for vaccine delivery, gold[92] and carbon[93,94] formulations are also studied. These materials are easily fabricated into unique shapes including cubes, rods, tubes and mesoporous spheres[92–95]. Further their surfaces are easily functionalized. Silica based systems also have some popularity due to their biocompatibility. Mesoporous silica particles are especially promising due to their adjuvant like properties, superior release kinetics, and they can be degraded and excreted[96,97]. These inorganic formulations are typically less common than other degradable materials, and the majority of systems reaching clinical trials tend to be liposomes[95].

Nanoparticles and other nano systems offer great promise for the next generation of therapies, and prophylactic strategies. This unique platform offers control over biodistribution, bioavailability, and biocompatibility of many therapies. Improvements that could save lives, money and improve the quality of life for patients suffering from many indications like cancer or chronic pain. Therefore, it is critical to continue research into these systems. While nanomaterials demonstrate great promise in drug, gene, and vaccine delivery, there are still many hurdles still face nanoparticle systems, such as burst release of drugs, and toxic bioaccumulation. Continued research, and optimized design will allow us to both improve the positive aspects of nanoparticles such as their targeting and controlled release kinetics, while finding ways to overcome or utilize the pitfalls of the system.

2.2. Cell Behavior Probes

As we refine our understanding of cellular systems each new generation of questions becomes increasingly complex. This increasing complexity necessitates improvements in the tools we use to interrogate cell behavior. Unfortunately, due to the immense intricacy of living cellular systems many current mechanisms of cell behavior analysis can lead to unwanted artifacts and very few of the current methods allow for non-invasive long-term analysis of cell behaviors. This lack of tools becomes especially apparent at the single cell level. The need for a generation of tools that can increase the resolution of our imaging systems and detect even trace amounts of molecules is

critical. Fortunately, nanoparticles have shown promise in their exceptional ability to interrogate cells and diagnose illnesses.

Many classical techniques require cells to be fixed or lysed to understand what proteins, signaling factors, or genetic materials they are expressing. These techniques do offer excellent insight into the function and behavior of cells, however, the necessity to lyse or fix cells limits these tools to endpoint analysis. While endpoint analysis is crucial it limits our understanding of the behavior of cell, and requires us to assume that all cells in a population have similar behavior over all time. While there are techniques available to get real time imaging of these phenomena, such as genetically encoding expression of GFP, or its variants, these labeling procedures are typically complex, can label a small number of cells, and can have significant impact on cell behavior[98]. Simpler techniques to study cell viability such as staining with membrane permeant dyes are typically short lived with fluorescent half-lives of a day or less. Other procedures such as single cell western blots offer understanding of the expression of proteins through immunohistochemistry[99], and genetic barcodes exist that allow for cell lineage tracing. However, both of these techniques require cell lysis to get at the genetic or proteomic material inside the cell[99,100]. Conversely, Nanoparticle systems offer the ability to interrogate cells in real time. This has non-trivial implications for improving our understanding of their secretome, transcriptome, and other cellular events. Current developments in nano systems are creating unique opportunities for particles to be utilized in everything from, high throughput genetic screening[101,102], to biochemical sensing[102,103], and even to ultra-sensitive disease detection[102,104,105].

2.2.1. In-Vitro Cell Behavior Probes

The detection of biological or chemical agents has a critical role in medical science. Making The recent development of a nanoparticle sensor that can efficiently label a wide range of cells, with minimal impact on the cells behavior particularly promising[106]. Nano sensors are often produced by the encapsulation of derivatives of organic fluorophores or hydrophilic

oligonucleotides that can sense explicit molecular sequences[102]. These Nano sensors are capable of longitudinal analysis of cell protein production. One good example of this is the encapsulation of Calcein Acetomethoxy (CAM) into nanoparticles to produce a cell viability sensor. CAM is a dye that requires cleavage of the acetomethoxy group by intracellular esterases to fluoresce[107]. Since these esterases are typically not present in dead cells it makes it a good dye for the detection of cell viability. However, Calcein AM is a relatively short lived dye[108,109] limiting its applications for longitudinal studies without frequent reapplication. The system that was developed by Yeo et. al. demonstrated release of Calcein AM from PLGA nanoparticle for over 28 days. Further this group was able to demonstrate accurate cell viability tracking for extended periods of time with minimal loss of signal compared to free dye controls[106].

Similar work with Nano sensor platforms has been done in the detection of nitric oxide, a secondary messenger that has critical interactions with several neurological, immune and other physiological processes[106]. Yeo et. al accomplished this by the incorporation of 4-amino-5-methylamino-2′, 7′ -difluorescein diacetate (DAF-FM-DA) into PLGA NPs. DAF-FM-DA can be deacetylated by intracellular esterases to remove the diacetate functional group producing a molecule that fluoresces following binding to NO. Similar to the release of CAM nanosensors DAF-FM-DA nanosensors showed release over the course of 28 days. This was demonstrated by showing fluorescence in HUVECs which produce NO in response to bradykinin peptides[106]. While this group produced two excellent examples of nano systems that enable longitudinal tracking of small molecules and cell viability, other groups have produced comparable systems that can track, aminothiols[110], and alkaline earth metal ions[111].

Protein and peptide detection is another common use of nanoparticle sensors with quantum dot based systems showing promise. Mattoussi was able to leverage q-dots to create a system that could detect the proteolytic activity of a number of enzymes[112]. This was done by creating a FRET system by conjugation of a dye to quantum dots, in the presence of proteases the dye is cleaved

from the quantum dot changing the fluorescent signature of the particles. Similar FRET based strategies have been employed for the detection of avidin[113], and glycoproteins[114]. Other FRET strategies utilize fluorescent macromolecules for the detection of proteins with nanoparticles, one example utilized gold nanoparticles that were functionalized with poly(p-phenyleneethynylene) (PPE). The fluorescence of PPE is quenched by the cationic nature of the nanoparticle, and following competitive binding of proteins the PPE is released allowing fluorescence recovery[115].

So far discussion of Nano sensors has involved a series of small molecules encapsulated or conjugated to particles that fluoresce in the presence of a biochemical, or signaling agent. Nano sensors have also demonstrated success in detecting gene and nucleic acid expression. One such platform works by encapsulation of hydrophilic oligonucleotide sensors. Utilizing double emulsion systems to encapsulate the hydrophilic oligonucleotides in hydrophilic polymers creates nano-sensors capable of non-invasively detecting mRNA expression. This is a largely preferable method to current strategies for the transport of oligonucleotides through the cellular membrane. Such as bolus loading following electroporation, or using a transfection agent which can have cytotoxicity concerns. Once inside the cellular membrane the encapsulated oligonucleotides can bind to the target mRNA causing a separation in the 5' and 3' ends of the nucleotide. This separation restores a previously quenched fluorophore[106]. Other FRET based strategies for the detection of nucleic acids utilize gold nanoparticles to quench q-dots. In the presence of unlabeled complimentary nucleotides, the q-dots dissociate from the gold restoring fluorescence[116].

2.2.2. In-Vivo Cell behavior probes

Nanoparticle systems have also been utilized as diagnostic systems for a range of indications including microbial infection and cancers. They have proven successful at the detection of several pathogens including gram positive, and gram-negative bacteria. This was done by complexing an anionic PPE loaded carboxylate particle with three cationic gold particles to create a fret system that would recover its fluorescence in the presence of bacteria[117]. It was able to identify

at least 12 different microorganisms. Q-dots have also shown great use in the detection of bacteria when conjugated to antibodies that bind to microorganisms like salmonella typhimurium[118], giardia lambia[119], Escherichia coli[120], and other oral bacteria[121–124].

Due to cancer being the second most common cause of morbidity and mortality in the US, it is of course one of the primary targets for nanoparticle in-vivo cell tracking**.** Because cancer arises from the patient's own cells it complicates detection by both the innate immune system as well as the diagnostic tests that are clinically utilized. Current methods of detection such as MRI Imaging and cytology, are limited by low sensitivity or inability to detect the early stage tumor [105]. Histopathology while excellent at determining the malignancy of tissues requires identification of lesions pre-biopsy. This leaves a large market for early detection techniques. Several nanoparticle systems are being developed to improve contrast and resolution of imaging platforms[125–128] and these are discussed in chapter 2.3.1. Another modality for the early detection is utilizing nanoparticles to detect biomarkers correlated with cancer. This can include surface glycoproteins[129] or secreted proteins[130], as well as nucleic acids[131–133] and various carbohydrates[134]. This approach is limited by low concentrations of these biomarkers, patient differences in biomarker expression, as well as challenges associated with collecting and storing pre-diagnostic samples[105]. However, nanoparticle systems have shown promise at addressing the technical issues associated with early diagnosis. Q-dots are especially promising in the production of inexpensive, quick and tailorable assays with high selectivity and sensitivity. Several "sandwich"-type assays in which a biomarker is trapped to an antibody and then sandwiched between a second capture antibody conjugated to a fluorophore have been developed. These assays allow for rapid reads as well as greater throughput of samples[105]. However, these assays are limited by the high selectivity of these antibodies making it critical to know the detection target in advance. Conversely the high selectivity of this approach allows it to be tailored to many analytes and does not require time intensive wash or optimization steps. One example of this assay type utilizes q-dots to detect neuron specific enolase and

carcinoembryonic antigen, two widely studied biomarkers of cancer. The system reported by Li et al. had a detection limit of 1 nanogram per milliliter[135,136]. Another group was able to lower the detection limit to .625 ng/ml by replacing streptavidin beads with immobilized capture antibodies[137].

Significantly more work is needed before these diagnostic systems will be utilized clinically however the fundamental ground work for improved screening is being laid by various nanoparticle systems. Continued improvements in nanoparticles as cellular interrogation tools and diagnostic strategies will see them rapidly emerge as major players in future medical and research fields.

2.3. Nanoparticles for Biomedical Imaging

Nanoparticle systems are rapidly becoming one of the most powerful and versatile tools across a wide range of biological applications, one area where their impact is particularly paradigm shifting is on the field of biomedical imaging, which encompasses techniques ranging from fluorescent microscopy to MRI and PET scans. The desirable, tunable size of nanoparticles have dimensions on scale with commonly studied functional groups[138,139], further they exhibit extremely diverse and tunable magnetic[103,126], excitation and emission properties[140,141] as well as desirable surface chemistry properties[17]. Additionally, nanoparticles are often more biologically inert than their encapsulated or conjugated fluorophores[103,142], and offer improved bio distribution[15,16], improved brightness of the imaging agent[141,143], and improved trafficking of the molecules across previously impermeable membranes[139,144]. Because of these numerous properties, the exploration of nanoparticles for biomedical imaging has dramatically increased over the last decade.

2.3.1. X-Ray Imaging

X-ray imaging is one of the most common modalities used in clinical settings, and an excellent example of the impact of metallic nanoparticles on the field. Metallic nanoparticles,

especially those utilizing gold, have risen in popularity for the potential as x-ray imaging contrast agents. They exhibit excellent biocompatibility and reduced short term toxicity[145,146], as is the common trend for many Nano systems. Gold nanoparticles have superior physical density properties and absorption coefficients when compared with iodine, a common contrast agent in x-ray imaging. (gold 79(Z), 5.16 cm2 /g, 19.32 g/cm3 ; iodine 53(Z), 1.94 cm2 /g, 4.9 g/cm3)[142]. These improvements helped improve spatial resolution of the imaging system, making it possible to see blood vessels 100 microns or smaller. This level of resolution even allows for in-vivo vascular casting[146].

Gold is extremely appealing to other imaging systems as well, especially CT scanning, another imaging modality that utilizes x-ray techniques to produce a visualization of tissue density variations. For this purpose, the most significant advantage of gold nanoparticle contrast agents is the vastly superior circulation half-life compared to the commonly used iodine doped small molecules. Iopromide, a common CT contrast agent has a half-life on the order of less than 10 minutes, whereas Kim et. al. have demonstrated PEG functionalized gold nanoparticles for CT imaging with a half-life greater than 4 hours[147]. Further, gold nanorods conjugated to UM-A9 antibodies have demonstrated great success at enhancing the contrast of squamous cell carcinoma, and at increasing the contrast in head and neck cancers without the conjugated antibody[127].

2.3.2. MRI Imaging

Gold is not the only commonly used metal for biomedical imaging nanoparticles. iron oxide is another widely explored material. Similar to the previously discussed gold nanoparticles, iron oxide nanoparticles show sufficient biocompatibility when administered at low doses[148], excellent response to magnetic fields[142], and surfaces amenable to functionalization[125,149]. Most importantly for imaging modalities though is the magnetic responsiveness of iron oxide. They exhibit superparamagnetism, when the magnetization of sufficiently small particles spontaneously reverses due to temperature. As well as significant field irreversibility. these properties likely

arising from the size of system as well as the specific surface properties of the system in question[150,151]. These superparamagnetic iron oxide nanoparticles (SPION) are particularly appealing as T2 MRI contrast agents due to their large magnetic moments[152]. A significant number of groups have demonstrated improved MRI imaging of a variety of tumors using SPION particles[153–158]. In addition to making excellent contrast agents for MRI imaging of tumors cells labeled with SPIONS have been utilized to track cell migration[159,160].

2.3.3. Fluorescence Imaging

Quantum dots are a semiconducting nanocrystal typically made of functionalized cadmium sulfide, cadmium selenide or cadmium telluride that exhibit very interesting fluorescent spectrum and electrical properties[161,162]. When compared to other widely utilized dyes or proteins, quantum dots have excellent quantum yield and brightness 10 to 100-fold stronger than comparable organic fluorophores[163]. Further they demonstrate narrow emission spectrum, with broad absorption, making it easy to drive fluorescence as specific tunable emission maxima, and they have significantly improved fluorescence lengths compared to organic dyes. 5-100ns compared to 1-5 ns respectively[163]. And finally they demonstrate 10^2-10^3 less photobleaching the comparable fluorescent dyes[163]. Making them significant improvements for imaging applications. They can also be specially functionalized to target to specific intracellular proteins or macromolecules allowing them to be used for understanding cell pathways and processes[164,165]. Despite the numerous potential advantages of quantum dots, they do have a few significant drawbacks. One prominent hurdle is the quantum blinking phenomena. Quantum blinking is an intermittency in the photoluminescence of the particle. It is thought to arise from escaping photocarriers, which are electrical carriers that have been excited by light in a semiconductor, on the crystal's surface. Improvements in shell coatings have been shown to reduce these phenomena but they are still present[166]. Another extremely relevant, but little understood aspect of nanoparticles is there

degradation in acidic environments or environments containing small molecule free radicals[167,168]. This will be further explored in chapter 4.

Though nanoparticles are extremely promising as next generation contrast agents and fluorescent molecules, each system will take considerable optimization to ensure reproducible, high quality products, with optimization regarding size, surface functionalization, and material formulation, with each variable having significant impacts on the success of the system for its modality. Further improvements in targeting, and shielding to improve circulation half-lives, pharmacokinetics, and bio distribution will likely be the next key areas of research. However, if the rate of improvement that has happened over the last 2 decades regarding improved contrast and brightness continue we will likely see more of these systems emerge to market.

2.4. Material properties

As seen in the previous section the material chosen for imaging nanosystems has significant impact on its success as a contrast agent. Similarly, understanding of the materials utilized in the formation of DDSs and imaging particles offers great insight into the fundamental properties of the nanoparticles they make. In the following section, the materials utilized in nanoparticle synthesis will be discussed and the impacts of physiochemical features of materials on nanoparticle features will be examined.

2.4.1. Biodegradable polymers

Poly lactic-co-glycolic acid (PLGA) is one of the most common and widely utilized polymer families for biomedical applications like drug delivery nano systems and tissue engineering scaffolds. PLGA is a copolymer of poly glycolic acid and poly lactic acid. PLGA has shown potential for these applications for a wide variety of reasons. First and foremost it has desirable biocompatibility and it has been extensively researched leading to an existing FDA approval status[2]. Further, PLGA has significant, but variable mechanical strength determined by

molecular weight and inherent viscosity of the polymers utilized[169]. It exhibits tunable degradation rates based on the molecular weight of the polymers and the ratio of the co-polymers. Because PLA has methyl side chains it makes it is more hydrophobic than PGA. This means that increasing the ratio of PLA to PGA makes the copolymer more hydrophobic which slows it degradation in water. Degradation of PLGA is driven by hydrolysis of ester linkages and it erodes in a primarily bulk degradation pattern[2,170,171]. This ability to tune the degradation rate also allows for prolonged sustained drug delivery, as has been demonstrated by many recent studies[1,172,173]. In addition to its appealing physical characteristics, it is readily functionalized[174]. Many commonly available forms of PLGA will be capped with carboxylic acids allowing for simple EDC-NHS reactions to attach other surface peptides, polymers, antibodies or other functional groups. It is additionally possible to order other forms of PLGA that have different functional groups to address specific functionalization or surface chemistry requirements. Without modification PLGA exhibits a base negative surface charge making it possible to use electrostatic interactions to deposit layers of positively charged polymers such as poly-L-lysine[21,80,106]. The inherent negative surface charge of PLGA additionally helps to prevent undesirable toxic interactions with negatively charged cellular membranes[2]. Unfortunately, PLGA is not a perfect material as it can have issues with burst release of encapsulated drugs[1,175], and can have unexpected drug-polymer interactions[176]. Additionally, it can be difficult to ensure monodisperse production and scaling to commercial production with PLGA[177]. While none of these issues are impossible to overcome, the optimization process for nanoparticulate systems can be time intensive. Furthermore, PLGA is a hydrophobic molecule which makes it particularly attractive for the encapsulation of other hydrophobic molecules, but can result in increased challenge if the encapsulated product is hydrophilic[178,179]. This challenge can be overcome with water-oil-water double emulsions but typically results in a loss of encapsulation efficiency[179,180], often making it advantageous to turn to other polymers for the encapsulation of hydrophilic molecules.

While polyesters are extremely popular for drug delivery systems many do exhibit bulk degradation, which can be undesirable. Other polymer options such as polyanhydrides have been developed with a focus on surface degradation kinetics. This is driven by hydrophobic backbones slowing water penetration to the core of the sample while anhydride linkages are rapidly hydrolyzed. This means that the surface of the polymer degrades much more rapidly than water is able to penetrate[181]. One example of this is the commercially available Gliadel wafer. The Gliadel wafer is a polyanhydride scaffold for the delivery of chemotherapeutics for gliomas[182]. It has shown respectable improvements in survival, and the benefit of controlled release of encapsulated Carmustine has been demonstrated by its approval despite the significant toxicity remaining[182,183].

A few natural polymers have found niche use as biodegradable polymers. Derivatives of DNA, and proteins have both found use due to their low toxicity and favorable pharmacokinetics[181]. Polysaccharides such as heparin, chitosan, and chondroitin sulfate[184,185] as carriers have brought similar clinical benefits. Additionally, there is increasing interest in DNA or RNA segments as targeting motifs[186]. Aptamers of RNA are particularly valuable as they are smaller, cheaper, and less immunogenic than antibodies. DNA has also been used to synthesize drug delivery systems, and has been formed into several shapes, including nanoboxes[187], and nanotubes[70,186]. Nanoboxes are particularly interesting as they can be designed to open in response to a protein or oligonucleotide[187]. Finally, proteins such as GFP have been modified to be highly stable and capable of delivering DNA, siRNA[188,189], or other proteins[189], while also enabling tracking of the delivered cargo through GFPs natural fluorescence.

Despite the prevalence and properties of PLGA systems research groups are constantly searching for new and better polymer systems. One recently developed system is acetalated dextran, a form of a complex polysaccharide that has both cyclic and acyclic acetals present following the reaction of the parent saccharide, dextran, with 2-methoxypropene or 2-ethoxypropene[35,190,191]. The presence of these acetal groups provides preferable solubility profiles for AC-DEX compared to

dextran as well as acid catalyzed degradation[191]. AC-DEX, unlike its parent saccharide, is soluble in polar solvents and insoluble in water. Making the polymer ideal for traditional emulsion or double emulsion nanoparticle formulation techniques. Further in the presence of acid the acetal groups break down returning the molecule to its parent saccharide. It does have additional byproducts from its degradation pathway, most notably methanol, or ethanol depending on whether 2-methoxypropene or 2-ethoxypropene was utilized during its synthesis. This produces a molecule that has a degradation rate that is extensively tunable in both neutral and acidic environments[35,191]. The extensively tunable degradation rate is most likely a function of the ratio of cyclic to acyclic acetal groups on the molecule. The ratio of which can be easily manipulated by changing one simple parameter in the production step[35]. The longer the reaction occurs the more of the acetal groups will transition from acyclic to the more stable cyclic form. Recent studies have shown the ability to control degradation rates to 2 orders of magnitude using this simple modification process, with half-lives ranging from 16-minutes for AC-DEX 5, the number denoting how long the sample was allowed to react for, to over 1600 minutes (27 hours) for AC-DEX 1500, in PH 5 water. Further only the most rapidly dissolving forms of AC-DEX demonstrate any significant degradation rate in pH 7.4 water[35,88,192]. While this polymer does have incredibly attractive tunability of degradation, it can produce toxic methanol during its degradation. Fortunately recent advances to the system have developed a version that will degrade to dextran, acetone and ethanol, far less toxic byproducts[193]. Additionally, its rapid degradation in acidic environments such as lysosomes has been hypothesized to provide an osmotic gradient capable of bursting the lysosome. This phenomena is what is believed to give acetalated dextran its adjuvant like properties[192].

2.4.2. Metals.

Metallic based systems are another common strategy for nanostructures. Gold, Iron oxide, tantalum and other metals all have uses for imaging and delivery of therapeutics. Iron oxide particles make some of the best contrast agents for MRI imaging[152,154], and gold has shown great

use in both x-ray imaging[146,147] as well as uses in FRET systems with other fluorophores[113,194]. Unfortunately, in contrast to biodegradable materials metals based systems have issues with biocompatibility and toxicity[142,148]. It is not totally understood what causes this cytotoxicity though many theorize it arises from either inflammatory responses or increased oxidative stress[102,138]. The toxicity and activity of metallic nanosystems is dependent on everything from size, chemical and surface and structural properties. In fact, 10 nm sized naked iron oxide nanoparticles have been shown to provoke apoptosis of HUVEC within 24 hours of internalization[148]. Gavard et al. hypothesized this was likely driven by the oxidative stress pathways. Further they presented significant inflammation in lungs, liver, and kidneys of mice following a systemic tail vein injection[148]. Many strategies that coat these metallic particles in various biocompatible materials has demonstrated reductions in cytotoxicity. Metallic nanoparticles have been coated in dextran[195,196], DMSA, alkoxysilanes and bisphosphonates[195,197,198]. Dextran has shown respectable increases in both stability and biocompatibility of iron oxide nanoparticles [195,196]. PEG is another common surface modification that has been demonstrated to improve circulation times and colloidal stability[199].

unmodified gold nanoparticles do exhibit slightly less toxicity as compared to iron oxide particles. Still, there is a great deal of research being done to functionalize the surface of gold nanosystems. Typically speaking there is two strategies for the functionalization of these particles. Either ligand exchange to conjugate a stabilizing group or direct incorporation[142]. Ligand exchange methods use thiol containing biomolecules to replace the stabilizers that are used during synthesis[200]. Alternatively, EDC chemistry can be exploited to conjugate biomolecules using amino groups on the end of stabilizers[200–202]. In some cases, people have even demonstrated the generation of gold nano structures with tumor specific molecules physically or chemically incorporated into the nanoparticle. Though this can have dramatic effects on polydispersity, and particle size of the nanoparticles[203,204].

2.4.3. Liposomes

Liposomal systems are typically composed of bilayers of phospholipids and were first described as early as 1965[205], since then a number of these systems have been approved for clinical use. Early liposomal systems suffered from difficulty trapping some types of molecules, and serum proteins could affect drug release[206,207]. These issues were addressed by incorporating cholesterol, transitioning to a solid phase bilayer, and the incorporation of sphingomyelin[208–211]. Despite this drug loading and drug release is still heavily dependent on the encapsulated therapeutic. Liposomes have significant issues in the retention of hydrophobic drugs such as paclitaxel[207]. This can to some degree be overcome by creating transmembrane pH gradients[212]. Transmembrane pH gradients can be produced either through the encapsulation of buffers, or salts like ammonium sulfate[213]. This also allows for loading of drug following formation of the vesicle in a process called remote loading[213]. Remote loading is typically done with drugs that have primary, secondary, or tertiary amines and are weak bases such as doxorubicin[212]. Early liposomal systems also suffered from rapid clearance from circulation by many classical mechanisms. The initial attempts to resolve this issue involved blockading the MPS with large doses of unloaded liposomes, however the advent of PEG has dramatically improved the half-life of liposomes[205].

2.5. Nanoparticle Physical Properties

2.5.1. Size and Polydispersity

Perhaps the most defining characteristic of nanoparticle systems is their size, and incredibly significant differences in internalization kinetics, binding affinities, and bioaccumulation can arise from a difference of even a few hundred nanometers. For this reason, in the design and characterization of a new nanoparticle system it is critical to determine the size range that you want to achieve. Once the target size has been determined, the next step is to ensure that the particle production process is indeed achieving that size range with minimal polydispersity.

Size of nanoparticles has significant effects on the mechanism of cellular endocytosis. Particles less than 60 nm will tend to be internalized though caveolin dependent endocytosis. Whereas particles around 100 nm will undergo either clathrin dependent or independent endocytosis. Particles 1 micron or larger will often undergo macropinocytosis or phagocytosis depending on formulation[151,214]. Size has noteworthy impacts beyond endocytosis mechanism, this property can affect permeation into tissues, location of bioaccumulation, as well as binding affinity of ligands. For example, extremely small nanoparticles, those less than 5-10 nm exhibit rapid systemic clearance through renal pathways[161]. Vascular fenestrations in the liver range from 50-100 nm which results in bioaccumulation of larger particles in the liver[215]. Larger micron scale particles, especially those in the 2-5 μm range will tend to accumulate in the capillary beds of the lungs and spleen[216]. Particles between 30 nm and 200 nm offer a good balance between circulation time and accumulation into tumors[217]. Control over the penetration depth and accumulation of particles in tumors can be modulated by control of the size of particles. 100 nm particles tend to remain trapped in the ECM near capillary walls, whereas smaller nanoparticles (20nm) offer excellent penetration but poor retention, often less than 24 hours[217–219]. Unfortunately, this means no single size can permeate, and accumulate sufficiently into all areas of a tumor lesion. Additionally, regardless of size tumor accumulation universally represents a small portion of total injected dose, typically between 1 and 10%[17].

Size has additional impacts on the functionalization of nanoparticle surfaces with it having direct effects on binding affinity of ligands. This phenomenon can be demonstrated by looking at the dissociation constant of Herceptin binding to ErbB2 receptor. Free Herceptin and 2 nm particles with bound Herceptin have a similar K_d of ~1.0×10^{-10}, larger 40 nm Her-NPs had a lower K_d of 4×10^{-13} article[220]. The increase in binding affinity is likely proportional to the changing size of the nanoparticle due to the higher density of proteins on the nanoparticles surface. Despite this, optimal internalization of particles is limited by the time it takes the membrane to engulf them, which is in

turn dependent on receptor diffusion across the membrane[220]. This means that for receptor mediate internalization particles in the 40-50 nm range have optimal balance between ligand binding affinity and internalization rate[220]. Mathematical modeling has demonstrated that this is likely due to their being no shortage of ligands or receptors in this size range[221].

Size is a critical aspect of nanoparticle synthesis and it can be quite difficult to achieve uniformity in nanoparticle size, especially in solvent evaporation methods. A metric of the range of sizes is referred to as polydispersity where the higher the polydispersity the larger the size range is of the particles[222]. While it is possible to filter out undesirable sized particles following nanoparticle formulation this can affect total particle yield. However, with careful control over the variables involved in the production process, ranging from sonication settings, to volumes of reagents, to time drying it is possible to painstakingly optimize procedures for production of nanoparticles. Optimization of size and minimization of polydispersity can become a much more daunting task when scaled up to commercial scale processing as uniform size and process efficiency become significant challenges[223,224]. Certain mechanisms such as flow focusing or electro spraying can produce improvements in the control of polydispersity or size, however, these processes are typically difficult to scale to commercial production[1].

2.5.2. Surface Charge

In addition to size, the surface charge of nanoparticles is another fundamental characteristic that can have significant impacts on both cellular uptake as well as bio-distribution. Due to the immense complexity of biological systems, it has rapidly become clear that even minor physiochemical differences in nanoparticles can have critical implications on the interactions between the particle and the target cells. To that end, recent studies have found that both the absolute value of the charge as well as the polarity of the charge effected uptake[151,225,226]. It was found that increasing absolute value of nanoparticles resulted in increased cellular uptake and that when controlled for absolute value positively charged nanoparticles tended to have greater

endocytic rates in phagocytic cells[225,227]. This changed a bit in non-phagocytic cells, as less negative particles, or increasing positive charge both related to increased uptake of nanoparticles[18]. Further, nanosystems with neutral or negative surface charge tend to hinder biofouling, which is the opsonization of foreign bodies by serum proteins. The reduction in biofouling has been shown to lead to improvements in circulation half-lives[144,216]. It has been shown that negatively charged NP result in lower accumulation in the spleen and liver when compared to neutral or positively charged NP[216]. Positively charged particles, especially cationic liposomes, have been shown to bind preferentially to tumor associated endothelium as well as sites of chronic inflammation[64,228]. In addition, positively charged particles have shown increased rates of endosomal escape, most likely through the proton sponge effect[229]. This dichotomy in the advantages of charge on particle bioaccumulation and uptake has led to significant increases in the design of environmentally responsive systems that can switch their charge at target locations. This is widely investigated for the treatment of tumors, as it is possible to leverage the acidic pH of the tumor microenvironment to produce charge changes[47].

2.5.3. Shape

Though the clear majority of nanoparticulate systems tend towards a spheroid structure, as that is the easiest structure to produce it is possible to create particles of differing shapes ranging from rods, to cubes and even more complex shapes. Just like charge and size this fundamental property of nano systems has significant impacts on cellular uptake, mechanism of movement through the blood stream and filtration systems of the body, as well as their *in-vivo* fates. Discher et.al demonstrated that filament shaped polymer particles had significantly longer half-lives when compared to standard spherical systems, on the order of 2-3 times as long[230]. This was further collaborated by demonstrating that rod shaped micelles exhibit circulation times 10 times longer than spherical micelles[230]. Further, Mitragori et.al demonstrated the impact of geometric parameters such as aspect ratio, and surface curvature directly impact macrophage internalization[3]. Their

results showed that spherical particles underwent faster internalization than non-spherical particles. However, other groups have shown that rods show superior uptake to spheres for particles greater than 100 nm[227]. In <100 nm range, many groups have demonstrated that spherical particles exhibit greater uptake[227,231,232]. This gave rise to the exploration of discoidal, cylindrical, and ellipsoidal particles that had minimal regions of curvature to enhance the accumulation of therapeutics in tumoral regions. Further research on these unique shapes is ongoing.

2.5.4. Surface Chemistry

As previously mentioned even minor physiochemical changes can have significant impacts on several aspects of the interactions between Nano systems and the target biological system. For this reason, the functionalization of nanoparticle surfaces is a widely-explored field, and many polymers, and other materials meant for nano systems now incorporate capping groups, capping groups are chemical structures that are typically reactive such as carboxylic acid groups or amine terminals, that allow for improved functionalization. The first step in discussing this aspect of nanoparticle design is to look at some of the common reactions used to attach functional groups to nano particle surfaces.

One of the most common, and simple mechanisms to add functional groups to the surface of a nanoparticle, especially polymer based systems. Is through an EDC-NHS reaction. EDC-NHS enables the rapid binding of carboxylic acids to primary amines. This reaction starts when EDC forms an active O-acylisourea intermediate following reaction with the carboxylic acid group. This intermediate is easily displaced by the primary amino groups through a nucleophilic attack mechanism. This results in an amide bond between the primary amine and the carboxylic acid group, with a soluble urea derivative byproduct being released. However, the time window in which this reaction can occur is a bit limited as the O-acylisourea intermediate is unstable. If no primary amine is present to complete the reaction, the carboxyl group is regenerated, and an N-unsubstituted urea is released. N-hydroxysuccinimide, or NHS is frequently included in the reaction to improve

efficiency, as it forms an NHS ester following coupling to the carboxyl group. This ester has preferable stability properties, and readily allows for conjugation to primary amines. The addition of NHS has the added benefit of allowing the reaction to occur efficiently at physiological pH rather than in acidic environment[233]. If this reaction is allowed to occur at pH 5 without the presence of NHS it can also be directed to conjugate carboxylic acid groups to a hydrazide moiety.

While NHS-EDC reactions are simple and excellent at conjugating primary amines to carboxylic acid there are a number of other functional groups that can be desirable. An excellent mechanism for this is the extremely stable biotin-avidin interaction. This conjugation method has been utilized for several nucleic acid and protein detection methods, as well as purification approaches. In addition, to the biotin-avidin interaction being the strongest non-covalent interaction between a protein and ligand that is currently known ($K_d = 10^{-15}M$), the biotin label is physically quite small meaning it typically has minimal impact on the function of the labeled molecule. Avidin is derived from avians and amphibians and shows remarkable affinity for biotin, which has roles in many biological processes across eukaryotes. Other forms of avidin do exist such as streptavidin, which is derived from the Streptomyces avidinii bacteria. Streptavidin does not have the glycosylation that avidin has making it more neutrally charged as well as decreasing nonspecific binding when compared to avidin. Neutravidin is a deglycosylated form of avidin that was developed to be more similar to streptavidin's charge and nonspecific binding. Further, the reaction is rapid and resilient to pH, organic solvents, denaturing agents, and even temperature[234]. While there are other mechanisms that can facilitate the attachment of functional groups to nanoparticles, these are two of the most commonly used reactions.

In the field of nano system drug delivery, one of the primary overarching goals Is long term sustained drug release. However, if the body is rapidly clearing these particles through the mononuclear phagocyte system (MPS), degradation rates are of little consequence. To that end, a major focus of research is how to extend the circulation half-life of nano-systems in vivo[22]. Early

methods of achieving this involved everything from massive dosing of empty liposomes to sterically hinder the MPS[235], to reduction of size of vesicles. While these had some positive impact on circulation persistence, they came with toxic side effects or limited efficacy[235]. Following these initial attempts, researchers began to investigate the differences between unmodified and modified particle surfaces. It was found that gangliosides conjugated to the surfaces resulted in significant improvements in circulation half-lives, as well as decreased uptake into the liver[20,134]. It was theorized that this was produced by the increase in the hydrophilic nature of the surface of modified liposomes[1,128]. The belief is that the increased hydrophilic nature was producing a shell of water molecules that was protecting the particle from serum protein adsorption. From there improvements in this approach have led to one of the most promising approaches for extending circulation time, the conjugation of polyethylene glycol, an extremely hydrophilic polyether polymer which showed substantial reduction in MPS clearance[19,216], and further had dose independent pharmacokinetics, except at extremely small doses. These new particle systems were largely termed "stealth liposomes" due to their ability to avoid clearance.

PEG is not the only strategy utilized to promote RES avoidance. Monosialylganglioside (GM1) is a similar molecule that is designed to help particles mimic the physical features of red blood cells. GM1 incorporates both the hydrophilic strategies that are highlighted by PEGylation as well as adding sialic acid moieties to the surface of liposomes. Sialic acid is a common moiety expressed on red blood cells and it has been demonstrated to play a role in the circulation times of red blood cells. Similarly, in liposomes incorporating GM1 it was found that RES clearance of nanoparticles was inversely proportionate to the ratio of GM1. Further GM1 modified liposomes demonstrated an impressive 25-fold increase in tumor accumulation as compared to unmodified liposomes. However, excess GM1 can destabilize liposomes, and its synthesis is challenging to replicate.

Several other polymers have been investigated for similar activity to peg such as poly-(acrylamide) (PAA), poly-vinyl pyrrolidine (PVP) and poly acryloylmorpholine. However, these polymers all expressed similar activity to PEG and showed little additional benefits. Because PEG exhibits favorable biocompatibility, easy synthesis, and is relatively cheap it is still widely preferred to these other polymers.

While conjugation of PEG or other hydrophilic moieties to nanoparticles is very common many nanoparticle systems will also conjugate ionic polymers to the surface to achieve a desired charge. Poly-L-lysine was previously discussed for playing a role in controlling the charge of nanoparticles as it is widely popular for this approach. Other similar polymers like poly ethyleneimine are strongly cationic and often used to modulate the charge of nanoparticles. PEI and PLL both have shown to facilitate endosomal escape as well as increasing interaction with cellular membranes. It is theorized that the cationic polymers like PEI and PLL function by creating a proton pump activity that lowers osmotic potential in vesicles. This decreased osmotic potential than drives an influx of water leading to swelling and bursting of endosomes.

2.6. Conclusion

This chapter has examined a wide variety of the fundamental properties of nanoparticles and discussed how these properties manifest into the appealing applications for medical therapies and tools. Understanding of the materials, and features of nanoparticles will help us to better develop new generations of therapies. In the following chapters, the methods of nanoparticle formation and particular protocols used in this thesis will be examined before transitioning to looking at how these properties combine to create novel platforms and the unique challenges that arise during the development of nanoparticle systems.

CHAPTER 3: METHODS

Nanoparticles are produced in a wide variety of methods including several methods that were not utilized during this thesis work. However, these methods still have distinct uses, and understanding of them is critical to understanding the production of nanosystems. Therefore, I will briefly discuss a few nano-formulation methods that were not utilized in this thesis. The principles of how they function and their advantages and disadvantages will be noted before moving on to the protocols that were utilized during this thesis. These protocols will be split into 3 sections relating to the project they were most utilized in.

3.1. Unutilized Formulation Strategies

Though these methods were not utilized during the course of this thesis work they are common approaches to making a wide variety of nanoparticle systems and therefore they will be explored briefly and their primary mechanisms will be examined before transitioning onto process performed during the course of this thesis work.

3.1.1. Microfluidic Nanofabrication

Microfluidic systems, while not used during this thesis work, are increasingly popular as means of scaling up production of monodisperse nanoparticles to commercial scales, and therefore worthy of discussion. This method focuses a polymer-solvent stream in the midst of an aqueous stream. This flow for these types of systems is almost always designed to have Reynolds numbers less than 20 and be purely laminar. This creates a highly controlled fluid regime which can reduce the physical, mechanical and chemical variation that can occur in emulsion based systems. By controlling the flow rate, and ratio of polymers-solvent phase to aqueous phase the size and polydispersity of created particles can be controlled. This is desirable in that it reduces batch to batch variation that can occur in other synthesis methods, however this type of process typically involves expensive machinery to model and then control fluid flows[236,237].

3.1.2. Spray Drying

Spray drying is another process not utilized during the course of this thesis that utilizes a heated gas to rapidly dry a liquid or slurry. This is a desirable way to produce dry powders of heat-sensitive pharmaceuticals. This process is desirable for creating consistent particle sizes which can be extremely valuable. Typically, oxygen is utilized as the drying gas, however in some cases where the solvent is flammable, or the product is reactive to oxygen, nitrogen can be used. Until recently this technique was limited to producing particles greater than 2 microns, and having low yield. Improvements in nozzle design, particle collectors and heating systems has reduced possible particle sizes to 300 nanometers with yields as high as 90%. These improvements are making spray drying an increasingly attractive option for the rapid production of monodisperse particles[238,239].

3.1.3. Electrospraying

Electrospraying functions similarly to spray drying, however, it utilizes electrical forces to atomize the liquid phase. This method for atomization also leads to highly charged droplets, which promotes dispersion by preventing coagulation. The size and charge of these particles is determined by the flow rate, and voltage of the system and Electrospraying can create nanoscale droplets. However, these systems are typically limited by low throughput and expensive equipment required to successfully create the flow and electrical fields necessary[240].

3.1.4. Nanoprecipitation

Nanoprecipitation is like solvent evaporation methods such as single and double emulsions; however, it utilizes a water miscible solvent. PLA can be utilized as a polymer of choice due to its hydrophobicity. The polymer is dissolved in a water miscible solvent added into an aqueous phase. This allows for the organic phase to rapidly diffuse throughout the aqueous phase causing the precipitation of a dissolved polymer. This technique is considered superior to solvent evaporation in some cases due to its ability to achieve high entrapment efficiencies and be relatively

monodisperse. However, it is a process limited to a few solvents that diffuse rapidly enough through water[241,242].

3.2 Barcode Project Methods

3.2.1 Cell Culture

Pre-characterized human MSCs (donors #00081 and #00082) purchased from RoosterBio were plated in mem-alpha that was fully supplemented with 15% fetal bovine serum (FBS) (Premium Select, Atlanta Biologicals) 1% L-glutamine (v/v), and 1% penicillin/streptomycin (v/v) at a density of 5000 cells/cm^2 unless specifically stated. Cells were lifted and passaged at approximately 70% confluence. Cells were not allowed to get beyond 80% confluence as this can lead to contact inhibition altering cell phenotypes. Cells utilized were between passages 4-6.

3.2.2. Single Barcode Preparation

This procedure was used to produce a batch of single color barcodes. 50 µl of anime latex beads (2%, 1um) were washed in filtered HBSS. Next .1 mg of EZ-link biotin is dissolved in 200 µl of filtered HBSS. The 50 µl of latex beads was then resuspended in the EZ-link solution and vortexed for 30 min @ power setting 4. The resulting particles were washed two times in 1% BSA supplemented HBSS before being resuspended in 50 µl of 1% BSA. A staining solution of 4 µl QD and 4 µl BSA was then made and mixed with the EZ-Link particles and allowed to react overnight. The final particles were then washed in BSA three times before being resuspended in 20 µl BSA.

3.2.3. Small Barcode Library Preparation

This procedure was done to produce a small library of ~27 unique barcodes. This process can be scaled up; however, this is infrequently necessary. 100 µl of anime latex beads (2%, 1um) were washed in filtered HBSS. Next .2 mg of EZ-link biotin is dissolved in 200 µl of filtered HBSS. The 100 µl of latex beads was then resuspended in the EZ-link solution and vortexed for 30 min @ power setting 4. The resulting particles were washed two times in 1% BSA supplemented HBSS

before being resuspended in 200 µl of 1% BSA. A staining solution of 14 µl QD and 56 µl BSA was then made for each QDd 625, QD 705 and QD 800. The staining solutions were then added to a 96 well PCR plate. The amount of each staining solution added to each well is described in the attached table. Following this 2 µl of EZ-link beads were added to each well of staining solution. The resulting conditions were placed on a shaker plate and allowed to react overnight. The final particles were then washed in BSA three times before being resuspended in 20 µl BSA. Finally, 100 µl of 1% (W/W) PLL was added to the particles to charge flip them.

Table 3.1: QD Ratios for Small Barcode Library

QD 625	**well 1**	**well 2**	**Well 3**	**well 4**	**well 5**	**well 6**	**well 7**	**well 8**	**well 9**	**well 10**	**well 11**	**well 12**
Row A	2 µl	4 µl	1 µl	1 µl	4.75 µl	1 µl	4.75 µl	1 µl	0.25 µl	0.25 µl	3 µl	5 µl
Row B	3 µl	5 µl	0 µl	0 µl	6 µl	0 µl	0 µl	5.5 µl	0.25 µl	0.25 µl	0 µl	1 µl
Row C	1 µl											
QD 705	**well 1**	**well 2**	**well 3**	**well 4**	**well 5**	**well 6**	**well 7**	**well 8**	**well 9**	**well 10**	**well 11**	**well 12**
Row A	2 µl	1 µl	4 µl	1 µl	1 µl	4.75 µl	0.25 µl	0.25 µl	4.75 µl	1 µl	3 µl	1 µl
Row B	0 µl	0 µl	3 µl	5 µl	0 µl	6 µl	0 µl	0.25 µl	5.5 µl	0.25 µl	1 µl	5 µl
Row C	0 µl											
QD 800	**well 1**	**well 2**	**well 3**	**well 4**	**well 5**	**well 6**	**well 7**	**well 8**	**well 9**	**well 10**	**well 11**	**well 12**
Row A	2 µl	1 µl	1 µl	4 µl	0.25 µl	0.25 µl	1 µl	4.75 µl	1 µl	4.75 µl	0 µl	0 µl
Row B	3 µl	1 µl	3 µl	1 µl	0 µl	0 µl	6 µl	0.25 µl	0.25 µl	5.5 µl	5 µl	0 µl
Row C	5 µl											

3.2.4. Barcode Uptake Procedure

This protocol was utilized to deliver intracellular barcodes and other nanoparticles to adherent human MSCs cultured as previously described. First cells were washed three times in covering volume -/- sterile PBS. Next serum deprived, non-supplemented media (mem-alpha-/-) with particles in desired ratio was prepped and added to washed MSCs. After 4 hours during which time the particles would associate with cellular membrane via charge interactions the media was supplemented with 4 ml mem-alpha with supplements. This stopped further particle association and provides resources for cells during internalization process. Cells were then incubated for 24 hours to allow for internalization of barcodes. Cells were then washed one time in -/- sterile PBS before being washed for 30 seconds in covering volume trypsin or acutase. This removed associated but none internalized particles. Finally, cells were washed two times in covering volume -/- sterile PBS before being utilized.

3.2.5. Fluorescence Microscopy

Particles were imaged on a motorized Leica DMI6000 microscope equipped with filters designed to excite and read Thermo Fisher's QD 625, QD 705, and QD 800. laser Intensity and exposure time were adjusted at the start of each protocol. All subsequent reads of the same particles were done using the same settings as previous acquisitions.

3.2.6. Morphological Change Tracking Protocol

This protocol was utilized to validate tracking of single cells over a time course and morphological change. Three color intracellular barcode labeled human MSCs were plated on Ibidi's μ-Dish with grid and optical glass bottom. Cells were imaged with fluorescent microscope and regions of interest were noted using the etched grid. Cells were then treated with 1ul/ml interferon-alpha in fully supplemented mem-alpha and allowed to incubate for 48 hours. Following incubation, the same regions of interest were imaged and barcodes were correlated between time steps.

3.2.7. Cellular Chemotaxis Assay Protocol

This protocol was utilized in the tracking of barcodes as cells migrated across a microfluidics chamber. The protocol was followed as written and provided by Ibidi. Passage 4 MSCs labeled with 3 color intracellular barcodes were seeded into the migration chamber and a gradient of fully supplemented to non-supplemented media was created in the wells. Plates were imaged on a Leica Inverted microscope after 0, 2, and 24 hours to visualize migration. Figure 3.1 contains an illustration of the microfluidics chamber utilized.

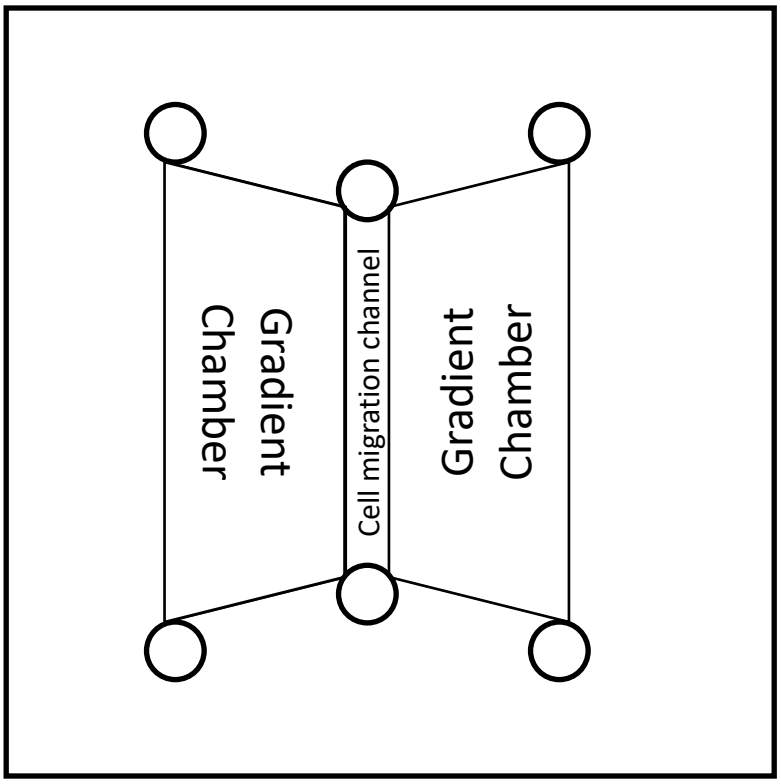

Figure 3.1: Ibidi's Microfluidic Chemotaxis Chamber.

3.2.8. Image Analysis: Barcode Intensity

Image analysis was performed using FIJI, an Image J based image analysis platform. This software could be used to manually or automatically select ROIs and then measure the intensity of each channel associated with that region of interest. This was used to read the fluorescent signatures of the barcodes.

3.3. Protocols used in the BAM 15 Project

3.3.1. Single Emulsion Nanofabrication

Single emulsion systems can be formed using two immiscible solvents, one of which the polymer is soluble in. In this project, the polymer was dissolved in a polar solvent such as DCM or DMSO. This solution is then mixed vigorously into a water bath where the polymer and polar solvent were immiscible. In order to improve the efficiency of this system and prevent the polar phase from forming into larger particles, an emulsifier such as PVA was added to the water bath to reduce particle interaction. The vigorous agitation of the emulsion is typically performed with either a probe sonicator or tissue homogenizer for larger particle sizes. After this the particles were placed on a stir plate and left to "dry" during which time the polar solvent evaporates away leaving the non-water-soluble polymer behind in the form of nanoparticles. These nanoparticles were than washed to remove the residual PVA, and finally either lyophilized for further storage or further functionalized through additional reactions. The following protocol is the final process determined to achieve 500 nm particles with good regularity. It was adapted from the protocol published by Ankrum et al. in Nature protocols 2014. First a 1% PVA bath was prepared by adding 200 mg of PVA to 20 ml of water. This process was done on a stir plate to ensure all PVA is dissolved, and can take up to an hour. Next 50 mg of 50/50 Poly(DL-lactide-co-glycolide) inherent viscosity .15-.25 dL/G was added to a scintillation vial along with 10 mg of BAM 15. 2 ml of DCM was then added to the glass scintillation vial containing BAM 15 and PLGA. When the PVA was fully

dissolved it was filtered using a .2 -µm filter., and placed on ice until chilled to less than 10 °C. Once the PVA solution was chilled the PLGA, BAM 15, DCM mixture was probe sonicated for 30 seconds to ensure homogeneity. The beaker of PVA was then placed on ice with the Probe sonicator submerged, but not touching any of the glass. while sonicating the PLGA, BAM 15, DCM mixture was added dropwise using a glass Pasteur pipette. Once all the DCM mixture was added the solution was probe sonicated for 2 minutes. Amplitude 20% with a 50 millisecond on 10 milliseconds of pulse. (for a Branson SFX150 µl trasonic Processor) were the settings utilized. The beaker containing particle suspension was then placed on a stir plate with a half inch stir bar. Before being covered with perforated parafilm and the stir plate was set to 300 RPM. Particles were allowed to dry for 12 hours before the particle suspension was added to a 50-ml conical tube and centrifuged at 5000 g for 5 min. Particles were then washed three times in distilled water to remove PVA before being resuspended in 2 ml of distilled water. Twenty µl of particle solution was set aside for zetasizing and the rest was frozen in preparation for lyophilization.

3.3.2. Size Measurement of Nanoparticles by DLS

Throughout the course of this thesis work the primary mechanism for quantifying the size of nanoparticle systems has been the use of Dynamic light scattering function of a Malvern Zetasizer. Dynamic light scattering (DLS) which is also called quasi-elastic light scattering (QELS) is a well-documented process to determine the size and polydispersity of nanoparticles and other sub-micron molecules that are suspended in a liquid. DLS works by measuring the intensity changes in scattered light as Brownian motion drives the movement of particles. This can then be used to calculate the size and polydispersity using the Stokes-Einstein relationship. The Stokes-Einstein equation correlates the size of spherical particles with their diffusion coefficient in a fluid with viscosity H at temperature T. N_A is Avogadro's Number and R is the gas constant. The Stokes-Einstein equation is as follows. $D=((R*T)/ N_A)*(1/(6*(pi)*H*A))$. Samples were prepared for size measurement by diluting 20 µl of sample into 1 mL of deionized water.

3.3.3. Zetasizing: Surface Charge Analysis

In addition to measurement of particle size by DLS, another important characteristic of particles is the zeta potential. Zeta-potential is a descriptor of the surface electrostatic potential of the system. This potential arises either from ionizable chemical groups on the surface of the molecule, or from the preferential adsorption of ions because of surface chemistry. It is important to note that though we refer to the particles as being charged, the solution the particle is dissolved in provides counter-ions to balance the charge. This produces a solution which overall is neutral, and because of the Brownian motion of the particles this field of counterions around particles is typically relatively diffuse. However, it is this relationship between the tightly bound ions on the particles surface and diffuse cloud of ions around it that help to facilitate the measurement of the zeta potential. Through the application of a charge, it is possible to drive motion of the particle via the bound ions, and by measuring the speed at which the particles move the zeta potential can be calculated. The speed of particle movement in response to an applied charge is the electrophoretic mobility (u_e) and is related to the zeta potential by the Henry equation (u_e) =(2*E*Z*F(k*a))/(3*n). where E=the dielectric constant, Z= the zeta potential, f(k*a) is the Henry function wherein k is the Debye parameter and a is the radius of the particle. N is the absolute zero-shear viscosity specific to the media chosen. This measurement can be indicative of a large number of fundamental properties of the system, ranging from probability of aggregation, to stability, and even viscosity of the solution. Samples were prepared for zetasizing by diluting 20 µl of sample into 1 mL of deionized water.

3.3.4. Lyophilization

Lyophilization, sometimes referred to as cryodesiccation, is the process of dehydrating a material through sublimation rather than evaporation. This process is driven by freezing a sample, and placing it under vacuum, moving the solution to a regime in which sublimation is a more energetically favorable process than melting and evaporating. Lyophilization is a critical process

in modern biology, as well as having implications for the storage and transport of many biological substances to this day. Lyophilization is a process in which a sample is first frozen, typically to a temperature between -50 and -80 °C, the sample is than placed under vacuum to move it below the substances triple point. Lyophilization is important in the preservation of many nanoparticle systems that incorporate biodegradable polymers as they will hydrolyze in the presence of water and slowly breakdown preventing long term storage, or transport. For other formulations of nanoparticles, such as liposomes, this procedure can be particularly tricky, and can result in the destruction of the nanoparticles. As such it is important to remember to evaluate the stability of any liposomal formulation following lyophilization or extended storage in a freezer.

3.3.5. Drug Loading Quantification

This protocol was utilized to determine the total amount of drug encapsulated in a given mass of particles. This could then be utilized to determine encapsulation efficiency. First .5 mg of BAM-15 PLGA nanoparticles were placed in a 1.5 ml centrifuge tube with 1 ml of methanol. Particles were then incubated for 1 hour on a 37-degree Celsius shaker to allow for complete release of encapsulated drug from PLGA. The solution was then centrifuged at 2,000g for 5 min to pellet the particles. The resulting supernatant was collected and Nano dropped to determine concentration. This could then be used to calculate the drug loading and encapsulation efficiency, examples of the formulas utilized are shown in figure 5.3

3.3.6. Release Kinetics Assay

This protocol was utilized to determine the degradation profile and release kinetics of BAM-15 encapsulated in PLGA. First a 5 mg/ml particle solution in PBS was prepared and added to a section of 14-kDA-MWCO dialysis tubing that was clamped shut at each end. This was then placed into a 50-ml conical tube with 20 ml of PBS -/-. Tubes were capped and placed on a 37 °C orbital shaker rack. 1 ml samples were removed at each time point, and 1 ml of fresh PBS -/- was

added every time a sample was removed. Once all samples were collected they were lyophilized and resuspended in methanol for nanodrop analysis.

3.3.7. Nanodrop

This protocol was utilized to measure the concentration of BAM-15 and other products released from nanoparticles. Nanodrop is a microvolume spectrophotometer that can measure absorbance or fluorescence. For this a Nanodrop 2000/2000c UV-Vis was utilized. 1 µl of sample was placed on the sensor and the absorbance of the sample was measured. Because of the small volumes utilized in this procedure evaporation of solvent can impact the read out, therefore to ensure accuracy between readings, the time that it took to start the measurement was set to 3 seconds, and only runs that were within +/- .5 seconds were used. Measurements were taken in triplicate.

3.3.8. NHS-EDC

This protocol was utilized to bind the brown adipose targeting antibody anti-P2Rx5 to carboxylate capped PLGA nanoparticles. The mechanism of NHS-EDC reactions is discussed in chapter 2, the protocol used was as follows. First 5 mg of lyophilized nanoparticles were added to 2 ml of prepared MES buffered pH corrected to optimal reaction pH. pH 6.3 MES buffer was utilized for the NHS-EDC reaction. Then .77 mg of EDC-HCL and 2.17 mg of Sulfo-NHS were added to the particle solution. This was allowed to incubate for 10 minutes. Following this 20 µl of targeting peptide at 1 mg/ml concentration was added to the solution. Reaction was allowed to occur on a shaker plate for 12 hours. Particles were then washed 3x in distilled water before being resuspended in 1 ml of sterile PBS-/-.

3.3.9. NHS-Hydrazide

This protocol was utilized to bind the white adipose targeting peptide to carboxylate capped PLGA nanoparticles. The mechanism of NHS-Hydrazide reactions is discussed in chapter 2, the protocol used was as follows. First 5 mg of lyophilized nanoparticles were added to 2 ml of prepared

MES buffered pH corrected to optimal reaction pH. pH 5 MES buffer was utilized for the NHS-Hydrazide reaction. Then 2.17 mg of Sulfo-NHS was added to the particle solution. Following this 20 µl of targeting peptide at 1 mg/ml concentration was added to the solution. Reaction was allowed to occur on a shaker plate for 12 hours. Particles were then washed 3x in distilled water before being resuspended in 1 ml of sterile PBS -/-.

3.3.10. Mouse Tissue Handling

All live mouse handling was done by Dr. Katie Markan PhD of the Pothoff lab at the University of Iowa in compliance with animal handling guidelines. C57BL6 breeder mice were used. A 200 µl injection of 5 mg/ml particle solution was systemically delivered to anesthetized mice via a retro-orbital injection. Following 24 hours the mice were sacrificed, dissected, and tissues were placed in a neutral buffered 10% formalin solution overnight. Following fixing tissues were washed 2x with distilled water, and imaged with a Licor Odyssey scanner

3.3.11. Licor Imaging

Fixed mouse tissues were placed in labeled 12 well culture plates and imaged on a Licor Odyssey Scanner for fluorescence in the 800-nm wavelength channel. DIR incorporated into nanoparticles systemically delivered to mice then fluoresced allowing analysis of bio distribution and bioaccumulation of modified and unmodified nanoparticles.

3.4. Protocols used while Assisting Other Projects

3.4.1. Double Emulsion Nanofabrication

While single emulsion systems are typically simple, they do have limitations in the encapsulation of hydrophilic biologics, as these drugs tend not to dissolve in the oil phase. However, one technique designed to overcome this limitation is a double emulsion in which a primary emulsion of water with drug in oil is created and then the primary emulsion is gently

agitated into another water path containing PVA. This produces a polymeric shell around an encapsulated aqueous center in which the hydrophilic drug or biologic is ideally encapsulated. This system does however have a few limitations. The primary emulsion of water in oil is typically fragile and easily broken, therefore the agitation that can be used to form the second emulsion is limited so that one does not break the primary emulsion. This typically means that particles produced using this technique tend to be quite a bit larger, typically on the micron scale. Additionally, it means a smaller portion of the particle can encapsulate drug thus leading to decreases in encapsulation efficiency and yield in some cases. The protocol was used to help develop a platform that could degrade themselves in a tightly controlled manner. Since AC-DEX's degradation is catalyzed by acid it was theorized that inclusion of Glucona-Delta-Lactone, a common hydrophilic food additive that becomes acidic upon protonation in water could be incorporated into AC-DEX particles to induce self-catalyzed degradation. First, A 1% PVA bath was formed by the addition of 200 mg of PVA to 20 mL of water. A second .1% PVA solution was made by the addition of 10 mg of PVA to 10ml of water. While the PVA solution is dissolving 50 mg of AC-DEX was added to a scintillation vial with 2 ml of DCM. Glucona delta lactone was then added to the .1% PVA solution, and the 1% PVA solution was filtered by a .2 -µm filter and placed on ice to chill. 1 ml of the .1% PVA/GDL solution was then probe sonicated into the AC-DEX/DCM mixture for 30 seconds at 50% amplitude. the tissue homogenizer was placed in the beaker of 1% PVA on ice and set to mix at a power setting of 8. The primary emulsion was then added dropwise to the 1% PVA solution while the tissue homogenizer was running. This solution was allowed to mix for 3 mins before a .5" stir bar was placed in the beaker and put on a stir plate set to 300 RPM. The beaker was then covered with perforated parafilm and allowed to dry for 4 hours. Following which the particles were centrifuged at 5000 G for 5 mins and washed 3 times to ensure removal of excess PVA. Particles were then zetasized and frozen for lyophilization.

CHAPTER 4. BARCODE PROJECT

4.1. Introduction

Single cell behavior is a critical component of a wide variety of both healthy physiological and diseased or dysfunctional micro-environments[243]. As such, it has become a major area of study in the scientific community. This is especially important in the study of regenerative medicine, tumor physiology and the role of stem cells in these therapies or indications[244–246]. Currently, the vast majority of tools used to analyze cellular behavior are unable to provide an adequate picture of cell populations. Most tools are designed to measure the behavior of populations as a function of the whole with little regard to the behavior of individual cells and unique sub-populations that exist in virtually every culture. Further, the few single cell techniques that do exist such as single cell microwells, signal cell RT-PCR, single cell western blot, microscopy, or flow cytometry are excellent though ultimately inadequate methods for understanding the behavior of single cells. Their limitation comes in their inability to repeatedly identify the same single cell in culture across time and space, meaning that each unique cell can only be effectively interrogated once. This approach to research is in direct contrast to the more nuanced approach we can take with larger more complex human or mammalian models in which each individual is able to be analyzed repeatedly over time. This type of analysis allows for deeper understanding of how outliers and unique individuals can affect the statistical behavior of the total as well as helping to identify specific indicators of predictive, or therapeutic outcome. These shortcomings motivated our attempt to develop a technology that could be truly paradigm shifting in the field of cellular research, the intracellular barcode. We hypothesized that using 800 nm microparticles we could develop unique identifying labels that could be delivered to whole populations of cells, a technology which would remove the need for a couple fundamental though flawed assumptions about cell biology. First that the measurement of separate cells from the same culture taken at different times are representative

of the behavior of the same cell in the population at different times, and relatedly that the average behavior of a culture is representative of all cells in that population.

4.1.1. Motivation and Current Techniques

Recent improvements in single cell analysis techniques have demonstrated the immense diversity in biological populations once believed to be relatively homogenous. Tools designed to analyze surface markers, secreted factors and the expression of genes of individual cells have been developed recently. Notable among these techniques is single cell RNAseq, developed by Tang et al[247]. and commercialized by Fluidigm™, which enables the sequencing of the transcriptome of a single cell. Single cell western blot systems have also been developed by Schaffer and Herr et al.[248] and commercialized by Protein Simple. Other techniques which are non-destructive such as flow cytometry, ELIspot or single cell microwells, and traditional microscopy, all allow for single cell analysis, however as previously mentioned, these techniques are only able to analyze a particular cell once.

Other cellular barcoding strategies have been developed in an attempt to enable repeat identification of cells along with spatial and temporal tracking. However, each technique has unique limitations that we theorized the intracellular barcode could resolve. Perhaps the most common current form of barcoding is DNA barcoding, a technique in which unique natural, or artificial sequences incorporated into a cell's DNA are used to identify a cell and its lineages[249]. This technique is limited to endpoint analysis only. This is due to the necessity to lyse a cell for its genome to be sequenced. Other techniques such as stochastic particle barcoding produced by Casterllarnau et al. are improvements over previous techniques and enable tracking between experiments. However, it is an extremely time intensive procedure and can be impractical when large cultures of cells need to be analyzed[250]. Further, this technique does not allow for analysis of any process that requires multicellular interactions. Nanoparticle vesicle encoding, another recently developed strategy works by introducing quantum dots to cells in sequence to produce a number of

colored vesicles in the cell. This does allow for live cell tracking and many other forms of analysis. However, it is unfortunately rather transient with codes typically only lasting 4-12 hours limiting analysis with this platform to short term applications[251].

As is clear, there is a need for a novel barcoding system. Such a system, capable of allowing identification in multicellular environments and accommodating of multiple single cell analysis techniques, could vastly improve our ability to repeatedly analyze cells. This could be paradigm shifting in our ability to understand the extreme complexity of cellular biology. Several sources have already utilized single cell analysis techniques to identify a number of sub populations in "purified populations" of cell types ranging from pancreatic beta cells to T-cells[245,252–255]. However, it is impossible to say if these are genuine sub-populations or merely transient states because we cannot re-interrogate the same cell. Better understanding of these states could help the scientific community to refine its efforts to therapeutic strategies that would have greater probabilities of working.

4.1.2. Approach

The Vision behind developing the intracellular barcode borrows from its predecessor NVE. However, where NVE utilizes the boundaries of the cell as the code area, we hypothesized that we could reduce the code to a single microparticle. This would allow us to create a less transient barcode whose entire fluorescent signature was limited to 1 pixel. a platform that could enable serial interrogation, across multiple analysis techniques and in complex multicellular environments.

To that end, we came up with a series of criteria that we needed to achieve to realize this system. First, the system had to be able to give individual readable signatures, preferably with large code depth to enable labeling of significant cell populations. Secondly, it needed to be compatible with complex environments in which multiple cell types are present. Third, it needed

to be stable and readable for a period over which repeat interrogation was possible, preferably a time scale in which lineage tracing would be possible. Finally, it needed to have minimal impact on cell physiology to maintain high quality analysis across a variety of single cell analysis techniques. In order to achieve these goals, we hypothesized that delivering 1 µm particles, which have been shown to be stable in MSCs for non-trivial periods of time[17,216], would be the optimal approach. By embedding or encapsulating different color quantum dots we could create a large library of fluorescent signatures that could be identified by traditional fluorescent microscopy.

4.2. Results

The first generation of barcodes produced in the lab was based on the conjugation of quantum dots to a non-degradable polystyrene core 800 nm in size. Given that most quantum dots are approximately 20-30 nm in diameter, this allowed for conjugation of roughly 3500 quantum dots to the cores. This was calculated by assuming the polystyrene particles modified with streptavidin were 1 micron in diameter giving them a surface area of $3.14x10^6$ nm. If we then assume each quantum dot has a radius of 17 nm, enough to give even the largest quantum dots extra space between them we see that there is enough surface area to conjugate 3458 quantum dots this was rounded up to 3500. Because the intensity of fluorescence in each channel increases in relationship to the number of quantum dots of a given color conjugated to that core we determined that by controlling the number and ratio of QDs we could create a large library of codes. Further, QDs primarily absorb light in the UV spectrum and have significant fluorescent shift avoiding the potential of FRET or quenching interactions[163]. Streptavidin conjugated quantum dots are available through Life Technologies, enabling a straightforward conjugation of QDs to a biotinylated core. This made them an ideal fluorophore with which to develop this technology. The first experimental procedure to validate our ability to control the number of QDs conjugated to particles and produce unique fluorescent signatures was to titrate the relative molarities of two quantum dots, QD 625 and QD 525, in the presence of biotinylated polystyrene cores. The results produced by Anthony

Burand, a Ph.D. candidate in the Ankrum lab, demonstrated a variety of codes shown in Figure 4.1, validating the ability to control the intensity levels. While we could control the relative intensities of multiple quantum dots on a barcode there was initially difficulty producing single color barcodes of lower intensities. This was because the streptavidin conjugated cores were aggregating as a result of open binding sites. In order to overcome this interaction, the addition of a non-fluorescent gold nanoparticle of similar size to the quantum dots was used to fill the excess binding sites. This strategy demonstrated success at both producing single color barcodes of varying intensity, as well as resolving the aggregation issue. Using this approach, up to 3 different colors of quantum dots we were able to create a library of several hundred codes and up to a theoretical max size of a few thousand. A subset of these codes is displayed in figure 4.1.

A significant concern associated with measuring the fluorescent intensity of the barcodes is the stability of their fluorescent signatures. Therefore, following validation of our ability to produce a variety of unique signatures of barcodes, it became necessary to demonstrate they could be read repeatedly and correctly identified. As such we fixed our barcodes in a mounting reagent and repeated imaged them against a control of brilliant violet, the data presented in figure 4.2 validates that QD intensity is significantly more stable than that of brilliant violet (BV) with BV losing about 25-30% of its fluorescence over 72 hours. Further repeat reads of the barcodes showed low variance between reads with the coefficient of variance ~3%. This variance does prevent us from assigning each particle a specific signature. However, by sufficiently spacing the barcode intensities it is possible to assign each barcode a bin of values such that if its fluorescence changes slightly it can still be identified repeatedly. Optimization of the size and spacing of these bins would be key to maximizing the library size and clarity. Figure 4.2 contains data, which demonstrates the validity of utilizing a bin based approach.

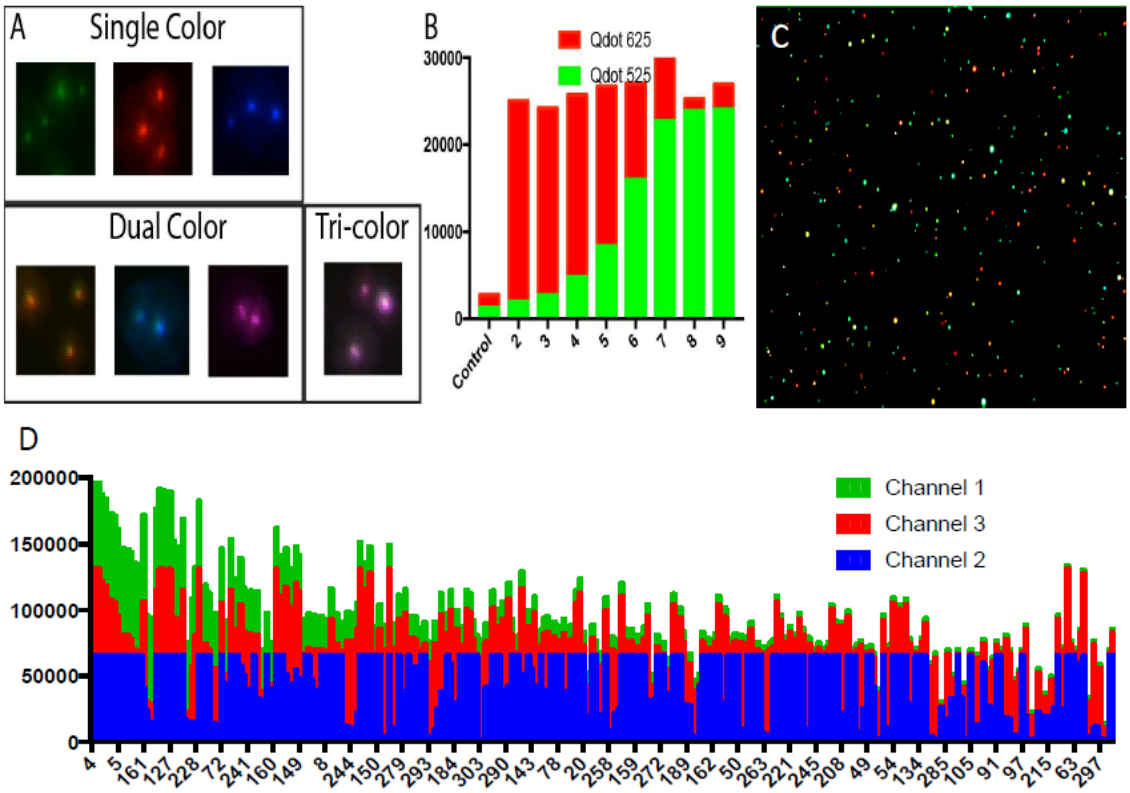

Figure 4.1: Barcode Library

(**A**) Fluorescence microscope images of select single, double and tri-color barcodes. (**B**) fluorescent intensity of dual 525,625 QD barcodes. With the contributions from each channel shown (**C**) Fluorescence microscope image of the small barcode library illustrates significant diversity of codes that can be achieved. (**D**) Variation in fluorescence of barcodes produced with the small barcode library protocol. The total contribution fluorescence from each QD channel Is illustrated.

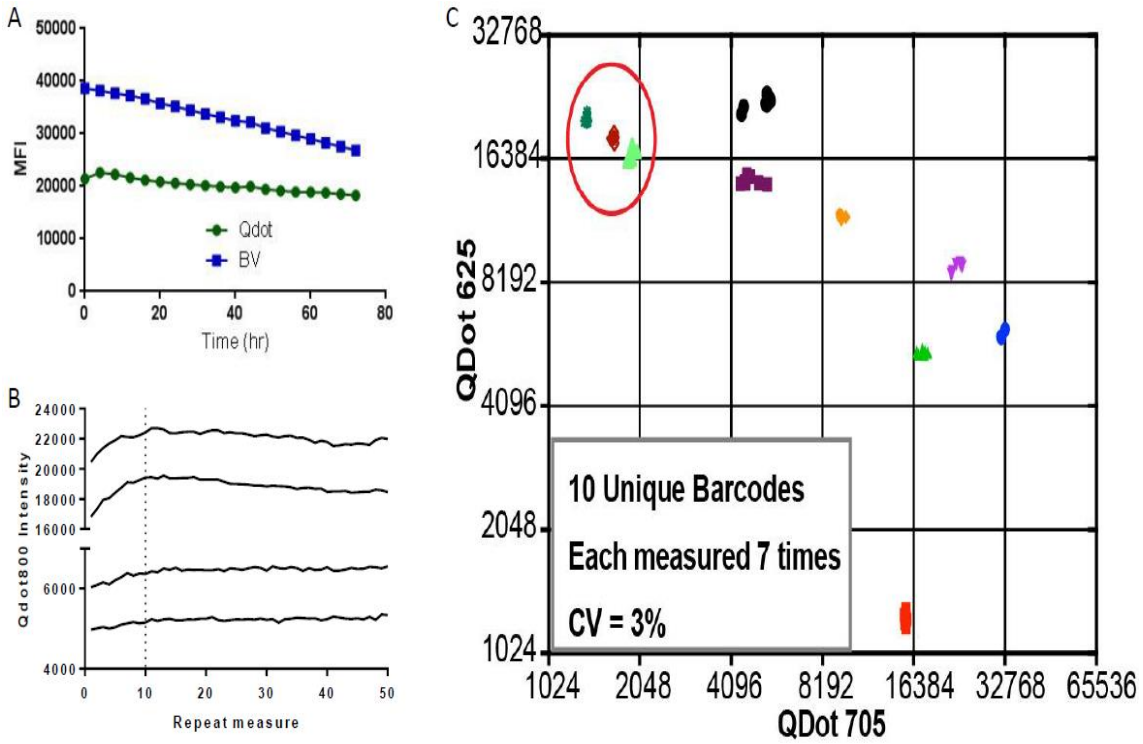

Figure 4.2: Barcode Stability and Binning

(**A**) Fluorescent microscope imaging of MFI of single color barcodes compared to particles with entrapped Brilliant Violet dye. Particles were fixed and imaged every hour. (**B**) Repeat fluorescent microscope measurements illustrate limited variation in barcode intensities (**C**) repeat reads of 10 unique dual color barcodes fixed in formalin. Barcodes show small variance however as can be seen by the 3 particles highlighted by the red circle even particles with similar intensities in both channels can be identified with no overlap. Adjustment of the size of bin used for each particles identity would be key to optimizing size of library.

To ensure rapid barcode internalization, barcodes were charge flipped by the addition of biotinylated poly-L-lysine. Biotin-PLL binds to excess streptavidin binding sites and flips the zeta potential of the particles from strongly negative (-30-40 mV) to strongly positive (+30-40 mV). This charge flip increases the likelihood of barcodes associating with and internalized into cells while having minimal observable impact on cell viability[63,173,216]. Z-stack imaging with deconvolution in figure 4.3 demonstrates validation of code internalization into cells. Further, once the barcodes are internalized, cells can be transported to new locations without altering the internalized barcodes.

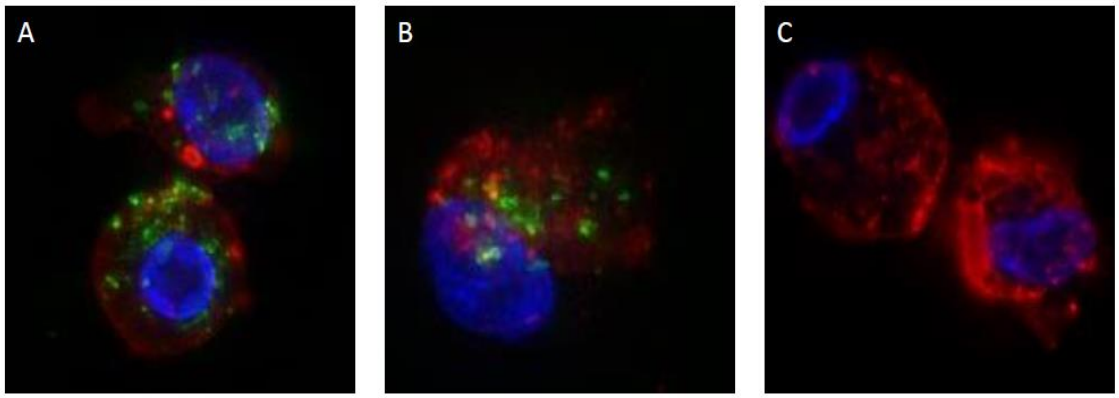

Figure 4.3: Cellular Barcode Internalization

Z-stack fluorescent microscope images with deconvolution. Human passage 4 MSCs were co-stained with Hoechst 33342 to stain the nuclei (blue) and DiO to stain the cellular membrane(red). Images (**A&B**) were labeled with 625 quantum dot barcodes (green) and image (**C**) was not been labeled with barcodes.

One significant problem that we encountered during this project was how to determine if a barcode had been transferred between cells. Commonly, if a cell underwent apoptosis it would release its barcode, allowing another cell to pick it up. If this occurred, it became impossible to determine which cell had died and which was the one that was still alive. To address this issue, we developed a system that could label or destroy particles that got released from a dying cell in parallel to the construction of the barcode library discussed above. We investigated several

potential mechanisms to drive this phenomenon. We considered including a cleavable moiety in the linker between nanoparticle and quantum dot, in which we looked at matrix metalloproteases and their ability to cleave collagen. However, it was hard to ensure that all quantum dots conjugated to a particle surface would be cleaved by the protease. Instead, we started to look towards utilizing dyes that do not penetrate cellular surfaces. Common examples of this include Propidium Iodide, a dye that fluoresces after intercalation with DNA; Calcein another common dye that is membrane impermeable fluoresces in response to either acidic pH or the presence of certain metallic ions such as zinc. Despite the wide variety of dyes available propidium iodide was chosen as the optimal dye for this system because we were able to find a biotinylated hexamers of nonsense dna that could easily be conjugated to our particles to make self-altering barcodes. Propidium Iodide, PI, has been demonstrated to intercalate every 4-5 bases[256]. This made hexamers of DNA good binding sites for the PI. Since PI is membrane impermeable, we could supplement our media with PI following incubation of cells with particles. This produced a system where cells that started with a barcode in them had barcodes that lacked the Propidium Iodide stain and did not fluoresce in that channel. However, if a cell were to die and release its barcodes they would pick up the PI dye and they could then easily be identified. Figure 4.4 demonstrates the successful labeling of these DNA conjugated particles. The self-altering of nanoparticles was seen to be robust and rapid. An average of Ninety percent of particles with the self-altering modification were labeled following a 5-min incubation in 1ul/ml PI in fully supplemented mem-alpha.

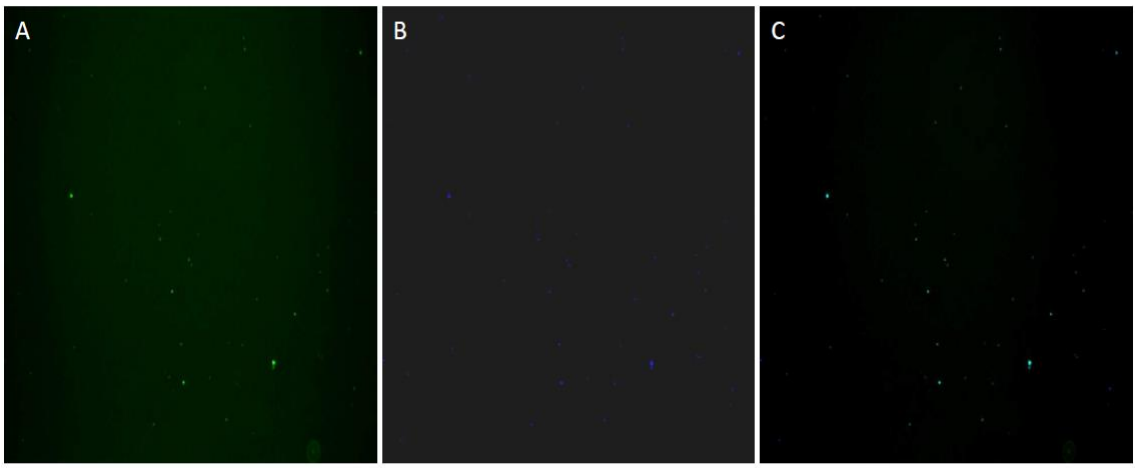

Figure 4.4: Self Altering Barcodes

(**A**) Fluorescent microscope image of self-altering barcodes in the QD 625 channel. (**B**) Fluorescent microscope image of same ROI of self-altering barcodes in the propidium iodide channel (**C**) overlay of both channels shows colocalization of PI and QD 625 channels

With several aspects of the barcode validated, including library size, fluorescent stability, ability of cells to uptake them in dose dependent manners, and self-altering in response to the environment, we moved to demonstrating functional utility. Our goal was to validate the tracking of live cells. The first experiment done utilized gridded petri dishes to provide, secondary, locational validation that the codes imaged were the same codes originally imaged. Interferon gamma was administered to the barcode labeled cells and their morphological change was visualized. MSCs have a well-documented morphological change in the presence of interferon. They tend to elongate and become more spindle-like[257]. Using locational data and the fluorescent signatures of the particles, we were able to re-identify them following a 48-hour incubation period. The cells were successfully identified, as can clearly be seen in Figure 4.5 they have become elongated, and more spindle like in classical fashion. This experiment also demonstrated a phenomenon that we hypothesized could happen. Namely that if a cell underwent mitosis the barcodes internalized into the cell would be split between daughter cells enabling generational tracking. This was determined to be lineage transfer because the two nanoparticles internalized to

one cell at the 0-time point were separated to two adjacent cells without either particle undergoing their self-altering process. Ultimately though despite being able to successfully identify cells over the course of 48 hours and identifying lineage transfer a significant complication was identified that will be discussed below.

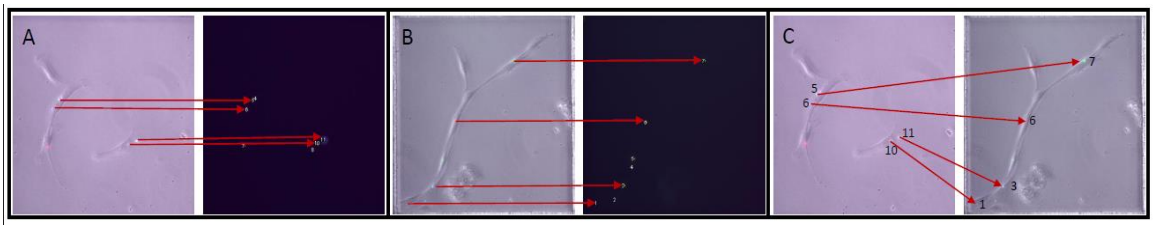

Figure 4.5: Morphological Change Tracking

(**A**) cells labeled with three color barcodes were plated on a gridded petri dishes and imaged to correlate internalized barcodes. Cells were then treated with 1ul/ml ifn-gamma. (**B**) Following a 48-hour incubation period the same ROI was imaged and the internalized barcodes were analyzed. (**C**) Barcodes were then correlated based on total fluorescent intensity and ratio of fluorescence between the 0-hour and 48-hour time points. Cells can be identified to have migrated, changed morphologically and undergone mitosis.

Parallel to this experiment an assay to demonstrate the ability to track the movement of cells was performed. Utilizing Ibidi's microfluidic cell migration assay, we plated barcode labeled cells into the chamber and created a nutrient gradient of FBS. The wells were imaged after 12 and 24 hours and the movement of the barcodes was analyzed. Ibidi states that their microfluidic cell migration assay is capable of holding a gradient for 48 hours. Unfortunately, we lacked a heated, or climate controlled microscope system. As such, we could not leave the culture in position on the scope, while every effort was made to ensure as similar of a plate setting between image acquisitions, it was impossible to ensure that each image was taken in the exact same location. In order to control for this, the displacement of each particle is measured relative to a common location in the wells. Figure 4.6 demonstrates the mechanism of measurement, and the displacement of the particles. FBS gradient did not provide significant migration of MSCs so the displacement of particles is limited.

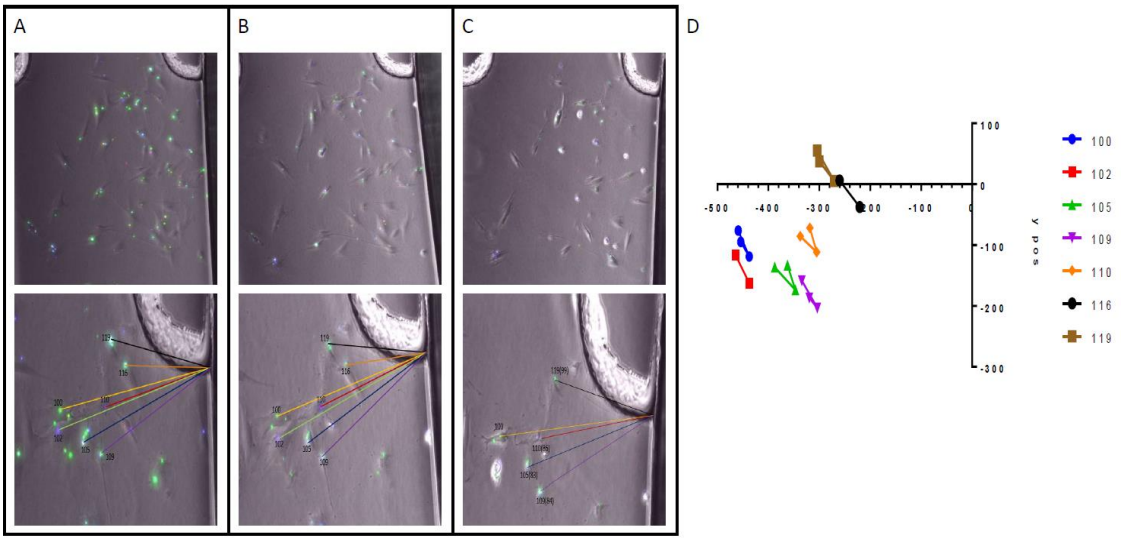

Figure 4.6: Cellular Chemotaxis Tracking

(**A**) Fluorescent microscope image of passage 4 human MSCs labeled with TRI-color barcodes plated into Ibidi's microfluidics chemotaxis platform. A gradient of 0% FBS supplemented mem-alpha to 15% supplemented mem-alpha was created to provide a nutrient gradient to drive chemotaxis. Barcode particles were given unique identifiers and mapped to an XY axis. The same process was done after (**B**) 2 hours, and (**C**) 24 hours. Barcode particles were then correlated based on total fluorescent intensity and ratio of fluorescence and their displacement was measured. (**D**) shows the XY displacement of each correlated particle.

4.3. Short Falls

While we were successfully able to repeatedly identify particles, during our functional tests we did identify a problem. The barcode signatures were rapidly decaying when inside cells. Figure 4.7 represents the decay of barcodes located within cells. This amount of decay far exceeded our expectations based on literature and in-house studies of quantum dot stabilities under ideal conditions. Further, the amount of decay made it very difficult to repeatedly identify most of the particles. Co-staining of labeled cells with lysosomal staining agents demonstrated that particles were largely localizing to lysosomes. This lead to the hypothesis that the harsh environment of the lysosome was rapidly degrading encapsulated quantum dots. Initial literature study indicated several potential mechanisms that could be driving the degradation. Some groups have shown that repeat or extensive excitation of quantum dots can slowly cause bleaching[258–260]. Other groups have

produced some evidence that demonstrated that alkaline environments could degrade the shell of the quantum dot causing loss of fluorescence[258,261]. These mechanisms were corroborated by in house testing that showed that the mean fluorescent index decreased in acidic media and when barcodes were excited by 425 nm light as opposed to 555 nm light. To determine if alkaline environments impacted barcode stability the particles were placed in either HBSS, a buffer that is stable at neutral pH, and in acidified media at pH 5 and imaged repeatedly. After 50 images of it was seen that barcodes in acidic Media had a MFI about 25 % lower than quantum dots in HBSS. A similar trend was observed in barcodes exposed to 425 nm wavelength light. After 50 exposures, the relative MFI was approximately half of its initial values and no significant changes were seen in barcodes exposed to 555 nm excitation. Figure 4.8 demonstrates the loss of fluorescence.

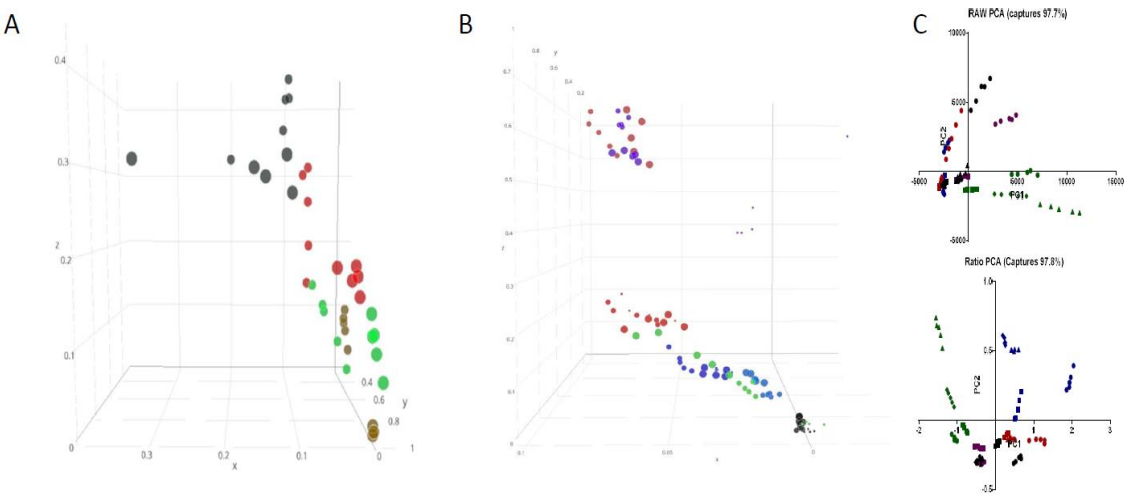

Figure 4.7 Barcode Degradation In-Vivo

(**A**) 3-d plot of quantitative fluorescent measurements taken of barcodes analyzed during morphological change tracking experiment discussed above. Time points of particles are shown by the size of points, large points are 0 hour measurements and small points are 48 hour measurements. Each color represents a unique barcode analyzed. Axis are the relative amount of fluorescence contributed by each QD channel, barcodes tend to degrade towards single color barcodes. Each barcode was read 5 times to account for possible variances (**B**) 3-D plot of quantitative fluorescent measurements taken of barcodes analyzed during the chemotaxis tracking assay discussed above. Large points are 0 hour and small points are 24 hour. Each color represents a unique barcode, and all barcodes were read 5 times to account for possible variance. (**C**) raw intensity and ratio of intensity primary component analysis performed. Each color is a unique barcode ● represents the 0 hour time point, ■ represents the 2 hour time point, ▲ represents the 7 hour time point, ♦ represents 24 hour time point.

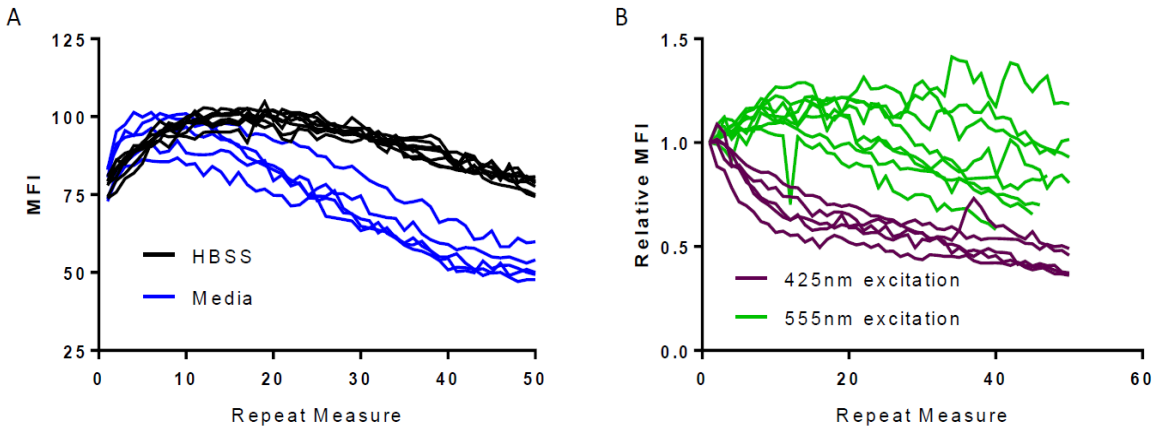

Figure 4.8 Barcode Decay In-Vitro

(A) Barcode particles were placed into either neutral HBSS or Media and imaged 50 times over the course of an horur. Their MFI was then plotted. (**B**) relative MFI of barcodes excited with either 425 nm wavelengths or 555 nm wavelengths during imaging. Each barcode was measured 50 times over the course of an hour.

4.4. Conclusion

While most of the characterization and design for this platform has proven successful, the decay of barcodes in the cellular environment is currently a significant hurdle. There are a couple of strategies, which could resolve this issue. First would be chemical inhibition of lysosome acidification or rupture of lysosomal vesicles via chloroquine or another agent. While this strategy offers potential to resolve the degradation, it was an approach we were opposed to as the addition of chloroquine, and other chemical agents could disrupt the natural behavior of cells in a way that we determined undermined the overarching goals of the project.

Another theorized strategy would be introduction of the barcodes to the cells via a non-endocytic pathway. Small particles have previously been demonstrated to be able to penetrate cellular membranes via simple diffusion mechanisms, which should theoretically allow them to enter a cell in a mechanism that would not locate them to a lysosomal vesicle. However, this strategy is limited because particles small enough to passively diffuse into cells can easily diffuse

back out. Additionally, particles in the size range where this is possible would be very limited in the number of conjugated quantum dots heavily limiting the size of the library. Strategies involving electroporation to produce internalization of particles have been tested. Unfortunately, electroporation caused degradation of the barcodes and can have impacts on cellular behavior.

Hopefully, continued research into stabilizing and functionalization of quantum dots will yield a particle that is stable in the lysosome. Fortunately, many groups are continuing research into these fields and recently some groups have presented evidence of new formulations for quantum dots that utilize polymers as opposed to metals[262–264]. These new highly fluorescent semiconducting polymer dots could present a platform that would enable the intracellular barcode technology. However, more research and characterization into these new polymer dots is needed before this approach could be practical. If these improvements can be demonstrated, any of these technologies could be rapidly and easily incorporated into the barcode platform. Success in this area would be a significant step in producing a photo stable, barcode capable of longitudinal single cell tracking.

CHAPTER 5: TARGETED DRUG DELIVERY SYSTEM FOR BAM-15:

5.1. Introduction

Obesity is one of the most significant health epidemics of the developed world, and is especially prevalent in the United States. In fact, the CDC estimated that in 2014 a full 37.9% of the adult population over the age of 20 was obese, with an additional 32.8% of the population being overweight. Further, projections made by the CDC showed that more than half of all adults will be obese by 2030. 20.6% percent of teenagers, and 17.4% of children aged 6-11 are also obese[265,266]. This represents a long-term health crisis across virtually every age, gender, and racial demographic. Obesity has been linked to a significant increase in the risk for heart disease, type 2 diabetes, stroke, a variety of types of cancer; many of these comorbidities are among the leading causes of preventable deaths. This health burden produced an estimated medical cost of 147 billion in 2008, with projections showing this cost could raise to as much as 390-580 billion annually by 2030[265,266]. Further, this estimated cost does little to calculate in the costs associated with lost time on jobs, and lost quality of life due to skeletomuscular issues that frequently arise in obese populations. While obesity is a major epidemic crossing many racial demographics, some groups are affected by it to a significantly higher rate; among these are non-Hispanic blacks who have a 48.1% age adjusted rate of obesity. Further, Hispanics also have an increased prevalence with 42.5% of the Hispanic population being obese[267]. As can be readily seen, obesity is a major health epidemic in the US. The most common non-dietary therapies for obesity are invasive, requiring cosmetic surgery or other more invasive procedures to reduce the volume a person can eat. Treatments for obesity also includes routine and behavior modification by promoting exercise and healthier diet. These changes can be challenging for the most widely affected demographics as low-income populations that have higher prevalence's of obesity often have inferior access to affordable healthy food or access to safe exercise facilities. This is a large part of the reason that obesity remains a long-term issue for the US.

5.1.1. Motivation

Because treatments for obesity are highly invasive, the possibility of developing a pharmacological therapy for obesity could have a massive long-term impact on the health of the general population. It could be especially impactful as a safer alternative to surgery with less post-operative recovery time necessary. Several pharmacological avenues to drive weight loss have previously been explored with one of the most effective being the use of protonophores such as 2,4-dinitrophenol (DNP). These protonophores function by disrupting the electron transport chain in mitochondrial membranes to make ATP synthesis by oxidative phosphorylation significantly less effective. DNP demonstrated a high degree of success at driving weight loss and was marketed as a diet aid between 1933 and 1938 before it was removed from the market. In addition to its dose dependent ability to increase basal metabolic rate, it could result in fatal hyperthermia if too much was taken. Moreover, many other dangerous side effects including seizures were prevalent as the drug would localize to the membranes of neuronal cells causing depolarization of the membrane[268]. Due to the dangers of this drug it is no longer considered a viable therapy for obesity, however it's mechanism of action as a protonophore has remained an area of investigation. Recent studies by Jastroch and Keipert et al. in 2013 discovered a similar protonophore, BAM-15 that maintained the uncoupling activity of DNP but lacked the cytotoxic side effects. By utilizing a patch-clamp technique they were able to demonstrate that BAM-15 was selective for the mitochondrial membrane and did not affect plasma membrane potential[269,270]. While this protonophore is very promising, our group was still concerned with minimizing the possibility of toxic side-effects while wanting to optimize the therapeutic value of a protonophore. As such we turned to our expertise in the development of Nano systems to design a controlled release, targeted nanoparticle. For this project, the following design criteria was decided on. First, we needed to identify what particle size range provided optimal targeting to adipose tissues following systemic delivery and then we needed to formulate BAM-15 particles in a size range capable of delivering drug for >4 days. Following

the initial discovery phase, extensive validation needed to be done to characterize and tune the release profiles and finally the identification of further targeting strategies to be able to target other depots such as brown adipose tissue.

5.2. Results

5.2.1. Initial Targeting and Size Range Determination

The first step was to determine the ideal size range of particles for delivery to adipose tissue. PLGA nanoparticles encapsulating the dye DIR ranging in size from 200 nm-1 micron were produced. Then the white adipose targeting peptide CKGGRAKDCGG with a 5000 kDa PEG spacer and hydrazide end group or a scrambled nonsense peptide of the same length were conjugated to the particles using an EDC reaction at pH 5. The scrambled nonsense peptide was a positive control to mimic charge and altered surface chemistry of targeted nanoparticles. Particles sized 200, 500 and 1000 nm were than systemically administered to mice via a tail vein injection. The mice were sacrificed and dissected after 24 hours and the fluorescence in the liver, spleen, epidydimal white fat and brown adipose tissue was examined. Figure 5.1 shows the relative fluorescent intensity of each of the organs as measured by odyssey scanner. It was observed that particles at the 500 nm size, with the attached targeting peptide, had the highest fluorescence and bioaccumulation in the epidydimal white fat. With a good white fat targeting peptide, and the appropriate size range identified the next step was to develop a process for engineering BAM-15 encapsulating nanoparticles via emulsion technique that reliably had a size distribution near 500 nm.

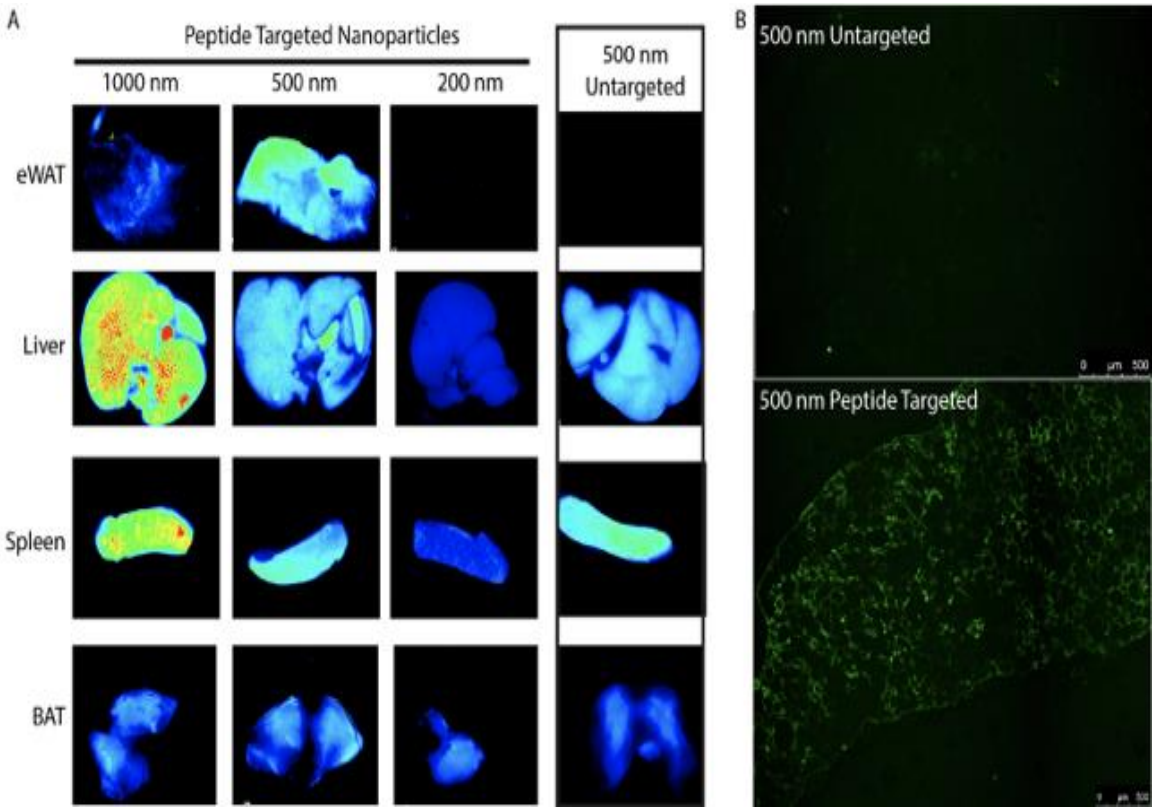

Figure 5.1: Biodistribution of Peptide Modified Nanoparticles in C57Bl6 Mice

(A) C57Bl6 mice were systemically injected with DIR loaded nanoparticles 200,500, and 1000 nm in size via tail vein injection. Mice were sacrificed 24 hours later and tissues were fixed in formalin. Tissues were Imaged on a LI-COR Odyssey Scanner and fluorescence intensity was mapped as a heat map. (**B**) eWAT tissue was sectioned and imaged with a fluorescence microscope. The 500 nm nontargeting peptide modified nanoparticle eWAT is compared to the 500 nm peptide targeted eWAT.

5.2.2. Process Engineering 500 nm Particles

Several parameters were investigated for their impacts on the final size and polydispersity of nanoparticles. Among these was surfactant concentration, increasing surfactant concentration should help prevent droplets of polymer-solvent solution from conglomerating. ratio of solvent to polymer, as well as the ratio of polymer to surfactant bath, were both analyzed to see how concentration impacted particle size. homogenizer speed and time, are strongly associated with homogeneity of mixing and size of particles produced. Similarly probe sonicator amplitude, time, and pulsatile mixing were examined. The amount of time the batch could dry for, as well as cooling of the drying bath were also studied. Nanoparticles formed via solvent evaporation can undergo a process called Ostwald ripening during the drying time in which the particles change size depending on time course and temperature. Finally, the loading of particles with dyes or drugs was investigated to see how addition of other components impacted particle size. Table 5.1 summarizes the general trends that were a result of each parameter. Figure 5.2 illustrates the process engineering approach that was taken and the sizes of chronologically ordered batches across the process demonstrates how we gradually moved towards a protocol that could produce 500 nm particles. Analysis of these parameters demonstrated that probe sonicator intensity, time, and pulse length had the most significant impact on particle size. As would be expected, increasing the power of probe sonication resulted in smaller particles. Increasing the length of time that particles were sonicated primarily reduced the poly-dispersity of particles. Finally pulsing the sonicator produced larger particles than continuous sonication. The exact procedure used is described in Chapter 3 page 39 under the heading “Single Emulsion protocol”.

Table 5.1: Table of Parameters in Particle Formulations and their Impacts on Size and Polydispersity

Modification	Change in Size	Change in polydispersity
PVA Concentration	Inversely Proportional	No trend observed
Ratio of DCM to PLGA	No trend observed	No trend observed
Ratio of PVA to DCM/PLGA	Proportional	No trend observed
Tissue Homogenizer speed	Inversely proportional	No trend observed
Tissue Homogenizer time	Inversely Proportional:	Inversely proportional
Probe sonicator intensity	Inversely Proportional-minor	No trend observed
Probe sonication time	Inversely Proportional	Inversely proportional
Pulsing of Probe Sonicator	Proportional	proportional
Temperature of PVA	No trend observed	Proportional
Methanol to DCM/PLGA	Proportional	Proportional
Loading particles with drugs	Proportional	Proportional

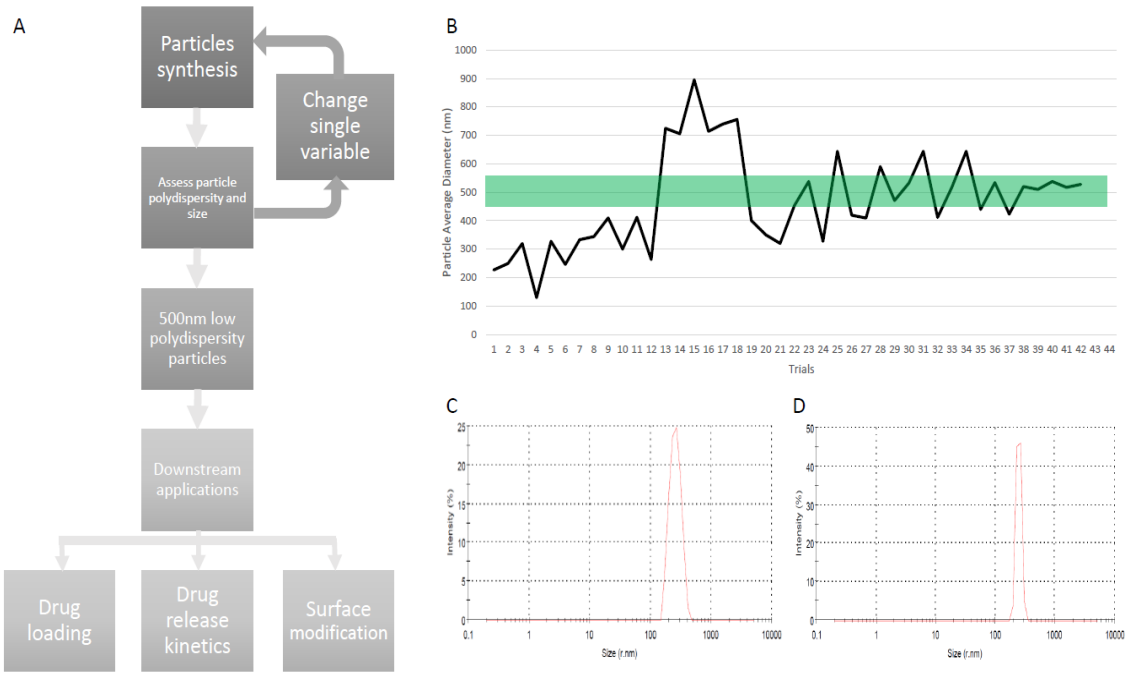

Figure 5.2: Process Engineering 500 nm PLGA Particles

(A) Flow chart illustrating the process utilized while developing the protocol to produce 500 nm particles with low polydispersity and characterize the resulting system. (**B**) Average diameter of chronologically ordered batches produced. The green highlight is the region where particles were 500 nm +/- 50 nm. (**C&B**) C and B are representative zetasizer results produced by the 500 nm protocol. The average radius of C is 517.8 nm and the average radius of D is 497.4. The width of the peak illustrates the narrow polydispersity achieved.

5.2.3. Characterization of Drug Loading

With a procedure for producing 500 nm particles, the next step became the characterization of the physical properties of the particles. As was expected, measuring the zeta potential of these particles showed that the particles were strongly negatively charged at -30 mV. This is primarily a result of using carboxylate end group PLGA, and indicates that the carboxyl groups are accessible to allow for post-production modification. Additionally, strong negative charge on nanoparticles is associated with a reduction in undesirable cellular interactions. Next the release kinetics, and drug loading of the particles was determined. BAM-15 absorbs at wavelengths of 205 nm, 230 nm, and 330 nm and a BAM-15 standard curve ranging from 5 μm to 100 μm for all 3 wavelengths was

constructed using nanodrop. Following this, to determine the drug loading, drug was released from 5 mg of particles using methanol to induce swelling of the PLGA. The resulting supernatant was isolated and analyzed by nanodrop. The absorbance was read at 205 nm, 230 nm, and 330 nm to determine the concentration of released BAM-15. This could then be used to calculate the total drug loading of the particles. It was found that on average batches showed a drug loading, the percent of particle by mass that is drug, of 7.5%. This further represented an encapsulation efficiency, the amount of BAM-15 added during the production process that was successfully encapsulated, of on average 60.4%. These are relatively standard encapsulation and drug loading values for this type of hydrophobic drug encapsulation in PLGA.

5.2.4. Characterization of Release Kinetics

With the maximum drug loading identified, we could start analyzing the release kinetics of the particles. To do this, 5 mg of nanoparticles were suspended in 1 ml of PBS and placed inside dialysis tubing. The dialysis tubing was placed in 20 milliliters of PBS in a 50-ml conical tube and placed on a heated shaker at 37 degrees Celsius. Samples were drawn at 4, 8,12, and 24 hours followed by taking a sample every 24 hours out to 10 days, lyophilized and resuspended in methanol. The resulting solution was measured by nanodrop and analyzed for concentration of BAM-15. The release are curves presented in Figure 5.3 are consistent with the type of PLGA that was used. A 10-day release curve was observed in which there was an initial burst release of ~20% of the encapsulated drug within the first 4 hours followed by a relatively linear release profile out to 10 days.

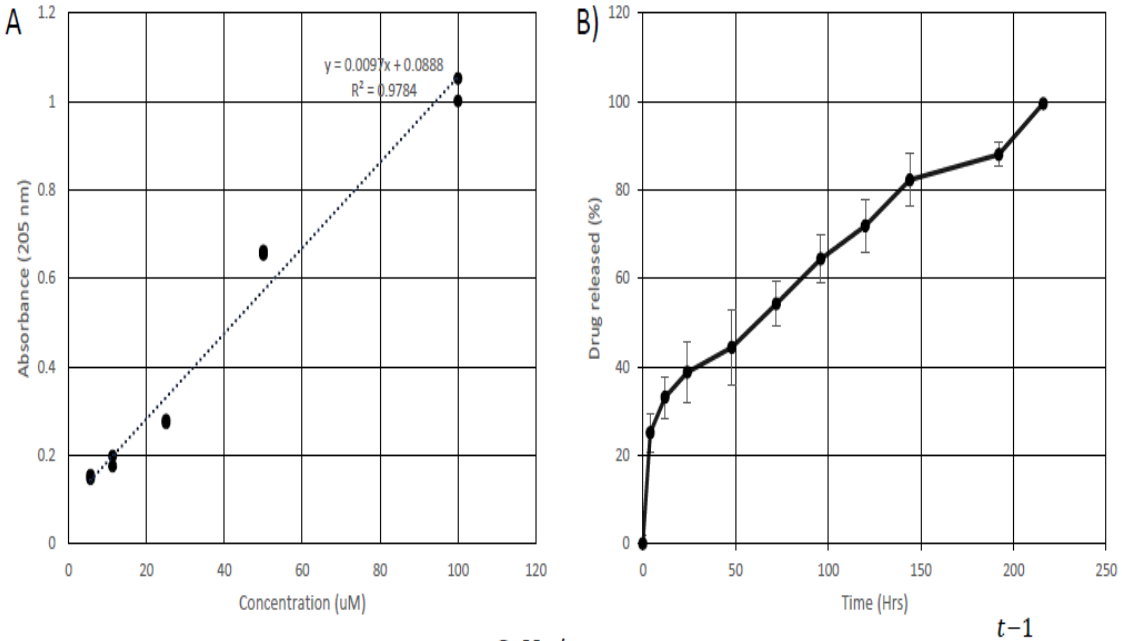

C) $\%DL = \frac{C_R V_R}{m_{mp}} x100$ D) $\%EE = \frac{C_R V_R / m_{mp}}{m_D / (m_D + m_{PLGA})} x100$ E) $CR_T = C_t V_R + \sum_{i=0}^{t-1} (C_t V_r)$

Figure 5.3: Drug Loading and Release Kinetics

(A) BAM-15 standard curve. Absorbance of BAM-15 as a function of molarity in methanol. Measurements made on nanodrop in triplicate, and time controlled. (**B**) Average BAM-15 release kinetics curve from PLGA, (n=5). (**C**) Formula used to calculate the percent drug loading of the particles by mass. C_r = concentration of release media, V_r = volume of release media, m_{mp} = mass of microparticles dissolved. (**D**) Formula used to calculate the encapsulation efficiency of the formulation process. C_r = concentration of release media, V_r = volume of release media, m_{mp} = mass of microparticles, m_D =mass of drug initially added during formulation, m_{plga} = Mass of PLGA initially added during formulation. (**E**) Formula used to calculate cumulative release at time T. C_t = concentration of the sample taken at time t, V_R = volume of release media taken at time t, C_i = the drug concentration at sample time i, and V_r = volume of release media taken at time i.

5.2.5. Targeting of Brown Adipose Tissue

The next step was to develop and further validate our ability to target to desired tissues as a means of reducing any potential off target effects, we decided to investigate a brown adipose targeting moiety anti P2rx5, an antibody to a receptor that is expressed predominately on brown adipose tissue[271–274]. The targeting moiety was attached to the particles through an NHS-EDC reaction in MES buffer at pH 6.3. In order to validate successful conjugation of the targeting peptide, zetasizing for zeta potential was done before and after the modification. Conjugation of the brown adipose targeting anti-p2rx5 resulted in a charge flip from -30mV to +16mV, further, conjugation of the white adipose targeting peptide resulted in a charge increase from -30mV to -0.5mV. This change in charge provided evidence of successful conjugation of the targeting moieties to DIR loaded particles. The Brown Adipose Tissue targeting particles, a control 500 nm particle and particles with the previously validated white adipose targeting peptide were systemically delivered to mice via a retro-orbital injection. 24 hours following injection the mice were sacrificed and dissected. The lungs, liver, kidney, spleen, heart, epididymal white adipose tissue, inguinal white adipose tissue, brown adipose tissue and the eyes were imaged by Odyssey scanner to detect fluorescence of the encapsulated DIR dye at the 800 nm wavelength. The resulting fluorescence is displayed as a heatmap in figure 5.4 along with the MFI for the adipose tissues as well as the liver and spleen. as you can see conjugation of the brown adipose targeting antibody had a similar impact to the white adipose targeting peptide. Increased accumulation is seen in every fatty tissue, though it is challenging to tell whether the BAT or WAT targeting moieties was superior. Both targeting peptides also show higher nonspecific accumulation in the liver and spleen, though bioaccumulation in the lungs, heart and spleen appear similar to controls. This could be the result of charge flipping of particles when the targeting moieties are bound. Increasing charge of nanoparticles would have impact on their uptake in all tissues. Additionally, the WAT targeting moiety has a PEG spacer. This PEG spacer would have likely decreased clearance of nanoparticles

leaving more to be imaged. The next step to test this hypothesis would be to administer mice with particles modified with a polymer such as PLL or PEI to determine what impacts charge alone has on uptake in adipose tissue.

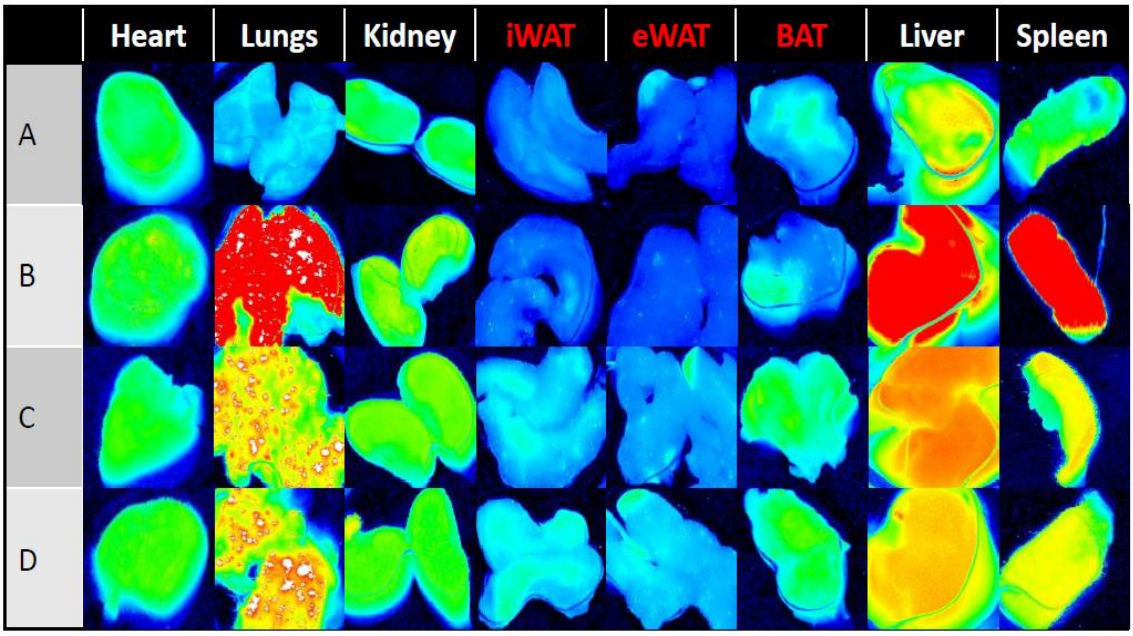

MFI	iWAT	eWAT	BAT	Liver	Spleen
A)	1	1	1	1	1
B)	0.98	1.01	0.98	3.64	5.01
C)	1.74	1.75	2.21	21.59	9.18
D)	1.59	1.37	2.70	21.80	6.33

Figure 5.4 Biodistribution of 500 nm Targeted Nanoparticles

C57Bl6 mice were systemically injected with 200 µl of 5 mg/mL DIR loaded 500 nm particles in PBS except mouse A which received empty PBS. 24 hours following injection mice were sacrificed and tissues were fixed. (**A**) empty control, (**B**) unmodified PLGA nanoparticles, (**C**) white adipose targeting peptide modified PLGA nanoparticles, (**D**) Brown adipose targeting antibody. Relative MFI for adipose tissues, liver and spleen are summarized in the attached table. MFI for each tissue is controlled relative to the MFI of the empty control mouse.

Chapter 5.3: Discussion

Despite other groups demonstration of metabolic activity and our own validation of respirational changes in cell culture when treated with BAM-15 with SEAHORSE, mice given 1 mg/kg injections of free BAM-15 failed to demonstrate any significant decrease in weight after 3 weeks in thermoneutral cages. Additionally, there was no significant change in gene expression or proteome. While it could be possible that 3 weeks is not adequate time to see a weight loss, perhaps systemic injection of free drug is rapidly cleared before it can affect tissue. This is still an unfortunate hurdle to the application of BAM-15 as a weight loss drug. however, BAM-15 has specifically been shown to be protective against renal ischemia and reperfusion injuries[270]. Other protonophores have been shown to have beneficial impacts on insulin sensitization and diseases associated with ROS production such as Parkinson's. As such, translation of this system to application in one of these indications could be possible.

Additionally, successful demonstration of targeting to white and brown adipose tissues opens the door to encapsulating different therapeutics in these particles for targeting fatty tissue in diseases where adipose tissue is defective. One possible disease state is diabetes, where adipose tissues shows chronic inflammation[275]. A classical marker of the chronic inflammation in diabetic fatty tissue is crown like structures produced by macrophages[276]. These macrophages are typically locked in pro-inflammatory phenotypes and express high levels of IL-1β and TNF-α[276]. Several small molecule inhibitors of IL-1β and TNF-α are available and good candidates for encapsulation in this platform, in addition more broadly acting steroids that are traditionally exceptionally easy to encapsulate in PLGA could be options. Either of these approaches could potentially demonstrate therapeutic value.

Despite these shortcomings this project did successfully develop a protocol to create 500 nm particles, a size range that could be desirable for several applications. Additionally, by highlighting the impacts of the formulation parameters a platform for future work has been laid.

This project also highlights some of the inherent difficulties in developing targeted nanosystems. While targeting might significantly alter the biodistribution it is not uncommon to see increased bioaccumulation in non-target tissues. These off-target effects can be challenging to manage and hard to predict due to the immense complexity of the body. Nanoparticles can fundamentally change how the body processes drugs and this could create issues. For example, as seen in the WAT and BAT targeting work done on this project increased bioaccumulation in the liver and spleen occurred, likely due to increased surface charge increasing non-specific tissue interactions. However, this could create unique challenges in prescribing such a therapy. Using this platform as an example, if a patient with a history of injury to the spleen wanted this therapy, a nano-formulation with these targeting moieties could potentially make the platform more toxic for them. Increased bioaccumulation in all tissues would need to be examined to determine the potential change in toxicological profiles and understand the patient populations it would be best for. This makes the next steps for this project determining whether it is charge interactions or reduced clearance due to PEGylation that is driving the increase in non-specific interactions and to examine tissues after exposure to drug loaded for evidence of any potential off target toxic effects.

CHAPTER 6: CONCLUSIONS AND FUTURE DIRECTIONS

The future of nanoparticle therapies and tools is very promising but ultimately dependent on developing systems that can scale to commercial manufacturing needs while maintaining uniformity and quality of the produced product.

Nanoparticles currently suffer from limitations in heterogeneity, burst release, and scaling to commercial production, however improving the techniques that we use to design and characterize these systems, and designing well optimized systems will help us to overcome these limitations. Improvements in production methods such as microfluidics and spray drying are opening the door to mass production of new types of monodisperse formulations. Further advances in targeting, and circulation time are helping to reduce the risk associated with burst release profiles. By targeting drugs to specific tissues systemic dose is reduced and burst releases are mitigated. However, further improvements in material design and environmentally responsive polymers should help to further refine control over this process making nanoparticle drug delivery systems safer and more effective. While these processes do require extensive and complex machinery to produce, improvements in storage of nanoparticles using lyophilization allows for mass production and distribution of shelf stable formulations. Off the shelf therapies are the gold standard of medical therapies as they require minimum preparation before they can be delivered to patients.

The work in this thesis for drug delivery nanoparticles focused on:

- Developing the production process for 500 nm drug loaded nanoparticles.
- Characterization of the encapsulation efficiency and drug loading of nanoparticles.
- Calculating the release kinetics of encapsulated biologics.
- Development of a targeting system that increases the concentration of nanoparticles in adipose tissue.

Unfortunately, BAM-15 lacked any noticeable effect in-vivo forcing us to rethink its application as a weight loss system. Fortunately, BAM 15 has been shown to be protective against IR injury, and other protonophores have been shown to improve insulin sensitization and protect against ROS associated damages that occur in aging and Parkinson's. these applications should allow for a seamless transition in the goals of project. The failure of BAM 15 to illicit a response in mice though does illustrates the necessity of testing the fundamental assumptions of any project. It also highlights how unexpected interactions can occur at any point in a project. This was further highlighted in a nanoparticle system developed for the Yang lab at the University of Iowa parallel to the work in this thesis in which an unpredicted drug polymer interaction spawned an idea for a new project. Observing the self-driven degradation of AC-DEX nanoparticles in response to an encapsulated biologic that was acidic was an unexpected drug polymer interaction that is now being leveraged to create a library of nanoparticle formulations that catalyze their own unique degradation profiles. Ideas like this could be the next step in developing environmentally responsive polymers.

This thesis also focused on a nanoparticle imaging tool designed to enable single cell tracking and repeat interrogation of individual cells. This project involved difficulties not frequently seen in imaging modalities that are typically limited by toxic bioaccumulation or biocompatibility issues. The degradation of QDs in response to the lysosome also highlights the limitations of what can be learned by reading published literature. The majority of papers discussing quantum dots laud their stability for both in-vivo and in-vitro applications, and very few mention their limitations. this could be a by-product of the current atmosphere regarding scientific publications. Very rarely is work done to confirm the work done by other groups, and even more rarely are papers published highlighting a failure. However, these failures are important aspects of understanding the world around us, and publication of failures could save time and money for other research teams with similar ideas. Despite the setbacks in this project

we were able to develop a tool that is on the verge of being able to cause a paradigm shift in cellular analysis. If improvements in quantum dot functionalization and design continue it is very possible that a lysosome stable barcode could still be developed. A platform for which we have already demonstrated the underlying functionality for.

Looking back over the work done during the past year in the Ankrum lab I have learned many things about material interactions, and the challenges that face us in the development of new systems. Most notably, the need to rigorously test the underlying principles of a project early on to validate the feasibility of the project, and the need for rigorous and detailed recording of all work done. Ultimately, I hope that I am able to take the lessons learned under the tutelage of Dr. Ankrum, and in the company of my peers in his lab to continue expanding our understanding of nano regime structures.

REFERENCES

1. Han, F. Y., Thurecht, K. J., Whittaker, A. K. & Smith, M. T. Bioerodable PLGA-based microparticles for producing sustained-release drug formulations and strategies for improving drug loading. *Frontiers in Pharmacology* **7,** 1853389–185 (2016).
2. Makadia, H. K. & Siegel, S. J. Poly Lactic-co-Glycolic Acid (PLGA) as biodegradable controlled drug delivery carrier. *Polymers (Basel).* **3,** 1377–1397 (2011).
3. Anselmo, A. C. & Mitragotri, S. Nanoparticles in the clinic. *Bioeng. Transl. Med.* **1,** 10–29 (2016).
4. Pisal, D. S., Kosloski, M. P. & Balu-Iyer, S. V. Delivery of therapeutic proteins. *Journal of Pharmaceutical Sciences* **99,** 2557–2575 (2010).
5. Mirza, A. Z. & Siddiqui, F. A. Nanomedicine and drug delivery: a mini review. *Int. Nano Lett.* **4,** 94 (2014).
6. Nakamura, Y., Mochida, A., Choyke, P. L. & Kobayashi, H. Nanodrug Delivery: Is the Enhanced Permeability and Retention Effect Sufficient for Curing Cancer? *Bioconjugate Chemistry* **27,** 2225–2238 (2016).
7. Wang, Y., Wei, X., Zhang, C., Zhang, F. & Liang, W. Nanoparticle Delivery Strategies to Target Doxorubicin to Tumor Cells and Reduce Side Effects. *Ther. Deliv.* **1,** 273–287 (2010).
8. Liu, Y., Tseng, Y.-C. & Huang, L. Biodistribution Studies of Nanoparticles Using Fluorescence Imaging: A Qualitative or Quantitative Method? *Pharm. Res.* **29,** 3273–3277 (2012).
9. Ndong, C. *et al.* Antibody-mediated targeting of iron oxide nanoparticles to the folate receptor alpha increases tumor cell association in vitro and in vivo. *Int. J. Nanomedicine* **10,** 2595–2617 (2015).
10. Nagy, J. A., Chang, S.-H., Dvorak, A. M. & Dvorak, H. F. Why are tumour blood vessels abnormal and why is it important to know? *Br. J. Cancer* **100,** 865–869 (2009).
11. Chen, F. *et al.* New horizons in tumor microenvironment biology: challenges and opportunities. *BMC Med.* **13,** 45 (2015).
12. Rink, J. S., Plebanek, M. P., Tripathy, S. & Thaxton, C. S. Update on current and potential nanoparticle cancer therapies. *Curr. Opin. Oncol.* **25,** 646–51 (2013).
13. Sykes, E. A. *et al.* Tailoring nanoparticle designs to target cancer based on tumor pathophysiology. *Proc. Natl. Acad. Sci.* **113,** E1142–E1151 (2016).
14. Bazak, R., Houri, M., El Achy, S., Hussein, W. & Refaat, T. Passive targeting of nanoparticles to cancer: A comprehensive review of the literature. *Mol. Clin. Oncol.* **2,** (2014).
15. Tsutsumi, Y. & Yoshioka, Y. Quantifying the biodistribution of nanoparticles. *Nat. Nanotechnol.* **6,** 755–755 (2011).
16. Kumar, R. *et al.* In vivo biodistribution and clearance studies using multimodal organically modified silica nanoparticles. in *ACS Nano* **4,** 699–708 (2010).

17. Albanese, A., Tang, P. S. & Chan, W. C. W. The Effect of Nanoparticle Size, Shape, and Surface Chemistry on Biological Systems. *Annu. Rev. Biomed. Eng.* **14,** 1–16 (2012).
18. Park, J. *et al.* PEGylated PLGA nanoparticles for the improved delivery of doxorubicin. *Nanomedicine Nanotechnology, Biol. Med.* **5,** 410–418 (2009).
19. Suk, J. S., Xu, Q., Kim, N., Hanes, J. & Ensign, L. M. PEGylation as a strategy for improving nanoparticle-based drug and gene delivery. *Advanced Drug Delivery Reviews* **99,** 28–51 (2016).
20. Suh, J. *et al.* PEGylation of nanoparticles improves their cytoplasmic transport. *Int. J. Nanomedicine* **2,** 735–741 (2007).
21. Van Vlerken, L. E., Vyas, T. K. & Amiji, M. M. Poly(ethylene glycol)-modified nanocarriers for tumor-targeted and intracellular delivery. *Pharm. Res.* **24,** 1405–1414 (2007).
22. Gref, R. *et al.* Biodegradable long-circulating polymeric nanospheres. *Science (80-.).* **263,** 1600–1603 (1994).
23. Kocbek, P., Obermajer, N., Cegnar, M., Kos, J. & Kristl, J. Targeting cancer cells using PLGA nanoparticles surface modified with monoclonal antibody. *J. Control. Release* **120,** 18–26 (2007).
24. Richards, D. A., Maruani, A. & Chudasama, V. Antibody fragments as nanoparticle targeting ligands: a step in the right direction. *Chem. Sci.* **8,** 63–77 (2017).
25. Chattopadhyay, N. *et al.* Role of antibody-mediated tumor targeting and route of administration in nanoparticle tumor accumulation in vivo. *Mol. Pharm.* **9,** 2168–2179 (2012).
26. Faraasen, S. *et al.* Ligand-specific targeting of microspheres to phagocytes by surface modification with poly(L-lysine)-grafted poly(ethylene glycol) conjugate. *Pharm. Res.* **20,** 237–246 (2003).
27. Kusminski, C. M., Bickel, P. E. & Scherer, P. E. Targeting adipose tissue in the treatment of obesity-associated diabetes. *Nat. Rev. Drug Discov.* **15,** 639–660 (2016).
28. Shohdy, K. S. & Alfaar, A. S. Nanoparticles targeting mechanisms in cancer therapy: current limitations and emerging solutions. *Ther Deliv* **4,** 1197–209 (2013).
29. Dinarvand, R., Sepehri, N., Manoochehri, S., Rouhani, H. & Atyabi, F. Polylactide-co-glycolide nanoparticles for controlled delivery of anticancer agents. *International journal of nanomedicine* **6,** 877–895 (2011).
30. De Jong, W. H. & Borm, P. J. Drug delivery and nanoparticles: Applications and hazards. *Int. J. Nanomedicine* **3,** 133–149 (2008).
31. Crasto, G. J. *et al.* Controlled bone formation using ultrasound-triggered release of BMP-2 from liposomes. *J. Control. Release* **243,** 99–108 (2016).
32. Torchilin, V. P. Multifunctional, stimuli-sensitive nanoparticulate systems for drug delivery. *Nat. Rev. Drug Discov.* **13,** 813–827 (2014).
33. Malhotra, V. & Perry, M. C. Classical chemotherapy: mechanisms, toxicities and the therapeutic window. *Cancer biology & therapy* **2,** S2-4 (2003).
34. Alnaim, L. Therapeutic drug monitoring of cancer chemotherapy. *J. Oncol. Pharm. Pract.* **13,** 207–221 (2007).

35. N, C. *et al.* Degradation of acetalated dextran can be broadly tuned based on cyclic acetal coverage and molecular weight. *Int. J. Pharm.* **512,** 147–157 (2016).
36. Hines, D. J. & Kaplan, D. L. Poly(lactic-co-glycolic) acid-controlled-release systems: experimental and modeling insights. *Crit. Rev. Ther. Drug Carrier Syst.* **30,** 257–76 (2013).
37. O'Brien, M. E. R. *et al.* Reduced cardiotoxicity and comparable efficacy in a phase III trial of pegylated liposomal doxorubicin HCl (CAELYX™/Doxil®) versus conventional doxorubicin for first-line treatment of metastatic breast cancer. *Ann. Oncol.* **15,** 440–449 (2004).
38. Waterhouse, D. N., Tardi, P. G., Mayer, L. D. & Bally, M. B. A comparison of liposomal formulations of doxorubicin with drug administered in free form: changing toxicity profiles. *Drug Saf.* **24,** 903–920 (2001).
39. Green, A. E. & Rose, P. G. Pegylated liposomal doxorubicin in ovarian cancer. *International Journal of Nanomedicine* **1,** 229–239 (2006).
40. Huebsch, N. *et al.* Ultrasound-triggered disruption and self-healing of reversibly cross-linked hydrogels for drug delivery and enhanced chemotherapy. *Proc. Natl. Acad. Sci.* **111,** 9762–9767 (2014).
41. Husseini, G. A. & Pitt, W. G. Micelles and nanoparticles for ultrasonic drug and gene delivery. *Advanced Drug Delivery Reviews* **60,** 1137–1152 (2008).
42. Mah, E. & Ghosh, R. Thermo-Responsive Hydrogels for Stimuli-Responsive Membranes. *Processes* **1,** 238–262 (2013).
43. Zardad, A. Z. *et al.* A review of thermo- and ultrasound-responsive polymeric systems for delivery of chemotherapeutic agents. *Polymers (Basel).* **8,** 1–22 (2016).
44. Junqiu Liu and Yanzhen Yin. Temperature Responsive Hydrogels:Construction and Applications. *Polym. Sci.* **1,** 1–6 (2015).
45. Traitel, T. & Kost, J. in 29–43 (Springer, Boston, MA, 2004). doi:10.1007/978-0-306-48584-8_3
46. Pohlit, H. *et al.* Biodegradable pH-Sensitive Poly(ethylene glycol) Nanocarriers for Allergen Encapsulation and Controlled Release. *Biomacromolecules* **16,** 3103–3111 (2015).
47. Gupta, P., Vermani, K. & Garg, S. Hydrogels: From controlled release to pH-responsive drug delivery. *Drug Discovery Today* **7,** 569–579 (2002).
48. Schmaljohann, D. Thermo- and pH-responsive polymers in drug delivery. *Adv. Drug Deliv.* **58,** 1655–1670 (2006).
49. Shen, S. *et al.* Near-infrared light-responsive nanoparticles with thermosensitive yolk-shell structure for multimodal imaging and chemo-photothermal therapy of tumor. *Nanomedicine Nanotechnology, Biol. Med.* **13,** 1607–1616 (2017).
50. Huu, V. A. N. *et al.* Light-responsive nanoparticle depot to control release of a small molecule angiogenesis inhibitor in the posterior segment of the eye. *J. Control. Release* **200,** 71–77 (2015).
51. Zhang, C. *et al.* A Light Responsive Nanoparticle-Based Delivery System Using Pheophorbide A Graft Polyethylenimine for Dendritic Cell-Based Cancer Immunotherapy. *Mol. Pharm.* **14,** 1760–1770 (2017).

52. Kretschmann, O. *et al.* Switchable hydrogels obtained by supramolecular cross-linking of adamantyl-containing LCST copolymers with cyclodextrin dimers. *Angew. Chemie - Int. Ed.* **45,** 4361–4365 (2006).
53. Gao, W., Chan, J. M. & Farokhzad, O. C. PH-responsive nanoparticles for drug delivery. *Molecular Pharmaceutics* **7,** 1913–1920 (2010).
54. Colombo, P., Sonvico, F., Colombo, G. & Bettini, R. Novel platforms for oral drug delivery. *Pharmaceutical Research* **26,** 601–611 (2009).
55. Dai, S., Tam, K. C. & Jenkins, R. D. Aggregation behavior of methacrylic acid/ethyl acrylate copolymer in dilute solutions. *Eur. Polym. J.* **36,** 2671–2677 (2000).
56. Vaupel, P. Tumor microenvironmental physiology and its implications for radiation oncology. *Seminars in Radiation Oncology* **14,** 198–206 (2004).
57. Griset, A. P. *et al.* Expansile nanoparticles: Synthesis, characterization, and in vivo efficacy of an acid-responsive polymeric drug delivery system. *J. Am. Chem. Soc.* **131,** 2469–2471 (2009).
58. Rapti, K., Chaanine, A. H. & Hajjar, R. J. Targeted gene therapy for the treatment of heart failure. *Canadian Journal of Cardiology* **27,** 265–283 (2011).
59. Pouton, C. W. & Seymour, L. W. Key issues in non-viral gene delivery. *Adv. Drug Deliv. Rev.* **46,** 187–203 (2001).
60. Robbins, P. D. & Ghivizzani, S. C. Viral Vectors for Gene Therapy. *Pharmacol. Ther.* **80,** 35–47 (1998).
61. Ponder, K. P. in *An Introduction to Molecular Medicine and Gene Therapy* 77–112 (2001).
62. Philippi, C., Loretz, B., Schaefer, U. F. & Lehr, C. M. Telomerase as an emerging target to fight cancer - Opportunities and challenges for nanomedicine. *Journal of Controlled Release* **146,** 228–240 (2010).
63. Dizaj, S., Jafari, S. & Khosroushahi, A. A sight on the current nanoparticle-based gene delivery vectors. *Nanoscale Res. Lett.* **9,** 252 (2014).
64. Kostarelos, K. & Miller, A. D. Synthetic, self-assembly ABCD nanoparticles; a structural paradigm for viable synthetic non-viral vectors. *Chem. Soc. Rev.* **34,** 970 (2005).
65. Mastrobattista, E., van der Aa, M. A. E. M., Hennink, W. E. & Crommelin, D. J. A. Artificial viruses: a nanotechnological approach to gene delivery. *Nat. Rev. Drug Discov.* **5,** 115–121 (2006).
66. Check, E. Gene therapy: A Tragic Setback. *Nature* **420,** 116–118 (2002).
67. Schwendeman, S. P., Shah, R. B., Bailey, B. A. & Schwendeman, A. S. Injectable controlled release depots for large molecules. *Journal of Controlled Release* **190,** 240–253 (2014).
68. Conde, J. *et al.* 15 years on siRNA delivery: Beyond the State-of-the-Art on inorganic nanoparticles for RNAi therapeutics. *Nano Today* **10,** 421–450 (2015).
69. Varshosaz, J. & Taymouri, S. Hollow inorganic nanoparticles as efficient carriers for sirna delivery: A comprehensive review. *Curr. Pharm. Des.* **21,** 4310–4328 (2015).
70. Ko, S. H., Liu, H., Chen, Y. & Mao, C. DNA nanotubes as combinatorial vehicles for cellular delivery. *Biomacromolecules* **9,** 3039–3043 (2008).

71. Zhang, Y., Satterlee, A. & Huang, L. In Vivo Gene Delivery by Nonviral Vectors: Overcoming Hurdles? *Mol. Ther.* **20,** 1298–1304 (2012).
72. Whitehead, K. A., Langer, R. & Anderson, D. G. Knocking down barriers: advances in siRNA delivery. *Nat. Rev. Drug Discov.* **8,** 129–138 (2009).
73. Guo, X. & Huang, L. Recent advances in nonviral vectors for gene delivery. *Acc. Chem. Res.* **45,** 971–979 (2012).
74. Knop, K., Hoogenboom, R., Fischer, D. & Schubert, U. S. Poly(ethylene glycol) in drug delivery: Pros and cons as well as potential alternatives. *Angewandte Chemie - International Edition* **49,** 6288–6308 (2010).
75. Davis, M. E. The first targeted delivery of siRNA in humans via a self-assembling, cyclodextrin polymer-based nanoparticle: From concept to clinic. *Molecular Pharmaceutics* **6,** 659–668 (2009).
76. Kanasty, R., Dorkin, J. R., Vegas, A. & Anderson, D. Delivery materials for siRNA therapeutics. *Nat. Mater.* **12,** 967–977 (2013).
77. Cui, Z., Han, S. J., Vangasseri, D. P. & Huang, L. Immunostimulation mechanism of LPD nanoparticle as a vaccine carrier. *Mol. Pharm.* **2,** 22–28 (2005).
78. Cui, Z. & Huang, L. Liposome-polycation-DNA (LPD) particle as a carrier and adjuvant for protein-based vaccines: Therapeutic effect against cervical cancer. *Cancer Immunol. Immunother.* **54,** 1180–1190 (2005).
79. Chen, W. & Huang, L. Induction of cytotoxic T-lymphocytes and antitumor activity by a liposomal lipopeptide vaccine. *Mol. Pharm.* **5,** 464–471 (2008).
80. Zhao, L. *et al.* Nanoparticle vaccines. *Vaccine* **32,** 327–337 (2014).
81. Couvreur, P. & Vauthier, C. Nanotechnology: Intelligent design to treat complex disease. *Pharmaceutical Research* **23,** 1417–1450 (2006).
82. Maurer, P. *et al.* A therapeutic vaccine for nicotine dependence: Preclinical efficacy, and phase I safety and immunogenicity. *Eur. J. Immunol.* **35,** 2031–2040 (2005).
83. Bovier, P. A. Epaxal ® : a virosomal vaccine to prevent hepatitis A infection. *Expert Rev. Vaccines* **7,** 1141–1150 (2008).
84. Herzog, C. *et al.* Eleven years of Inflexal® V-a virosomal adjuvanted influenza vaccine. *Vaccine* **27,** 4381–4387 (2009).
85. Kushnir, N., Streatfield, S. J. & Yusibov, V. Virus-like particles as a highly efficient vaccine platform: Diversity of targets and production systems and advances in clinical development. *Vaccine* **31,** 58–83 (2012).
86. Correia-Pinto, J. F., Csaba, N. & Alonso, M. J. Vaccine delivery carriers: Insights and future perspectives. *Int. J. Pharm.* **440,** 27–38 (2013).
87. Li, P. *et al.* Bioreducible alginate-poly(ethylenimine) nanogels as an antigen-delivery system robustly enhance vaccine-elicited humoral and cellular immune responses. *J. Control. Release* **168,** 271–279 (2013).
88. Broaders, K. E., Cohen, J. A., Beaudette, T. T., Bachelder, E. M. & Fréchet, J. M. J. Acetalated dextran is a chemically and biologically tunable material for particulate immunotherapy. *Proc. Natl. Acad. Sci. U. S. A.* **106,** 5497–502 (2009).
89. Feng, G. *et al.* Enhanced Immune Response and Protective Effects of Nano-chitosan-based DNA Vaccine Encoding T Cell Epitopes of Esat-6 and FL against Mycobacterium Tuberculosis Infection. *PLoS One* **8,** e61135 (2013).

90. Uenaka, A. *et al.* T cell immunomonitoring and tumor responses in patients immunized with a complex of cholesterol-bearing hydrophobized pullulan (CHP) and NY-ESO-1 protein. *Cancer Immun. a J. Acad. Cancer Immunol.* **7,** 9 (2007).
91. Hasegawa, K. *et al.* In vitro stimulation of CD8 and CD4 T cells by dendritic cells loaded with a complex of cholesterol-bearing hydrophobized pullulan and NY-ESO-1 protein: Identification of a new HLA-DR15-binding CD4 T-cell epitope. *Clin. Cancer Res.* **12,** 1921–1927 (2006).
92. Niikura, K. *et al.* Gold nanoparticles as a vaccine platform: Influence of size and shape on immunological responses in vitro and in vivo. *ACS Nano* **7,** 3926–3938 (2013).
93. Bianco, A., Kostarelos, K. & Prato, M. Applications of carbon nanotubes in drug delivery. *Curr. Opin. Chem. Biol.* **9,** 674–679 (2005).
94. Wang, T. *et al.* Synthesis of a novel kind of carbon nanoparticle with large mesopores and macropores and its application as an oral vaccine adjuvant. *Eur. J. Pharm. Sci.* **44,** 653–659 (2011).
95. Laura Peek, Middaugh, C. R. & Berkland, C. Nanotechnology in vaccine delivery. *Adv. Drug Deliv. Rev.* **60,** 915–928 (2008).
96. Zhai, W. *et al.* Degradation of hollow mesoporous silica nanoparticles in human umbilical vein endothelial cells. *J. Biomed. Mater. Res. - Part B Appl. Biomater.* **100 B,** 1397–1403 (2012).
97. Yamada, H. *et al.* Preparation of colloidal mesoporous silica nanoparticles with different diameters and their unique degradation behavior in static aqueous systems. *Chem. Mater.* **24,** 1462–1471 (2012).
98. Kim, T. K. & Eberwine, J. H. Mammalian cell transfection: The present and the future. *Anal. Bioanal. Chem.* **397,** 3173–3178 (2010).
99. Ghosh, R., Gilda, J. E. & Gomes, A. V. The necessity of and strategies for improving confidence in the accuracy of western blots. *Expert Rev. Proteomics* **11,** 549–560 (2014).
100. Burgess, D. J. Technique: Genome editing for cell lineage tracing. *Nat. Rev. Genet.* **17,** 435–435 (2016).
101. Zu, Y. *et al.* Nanoprobe-based genetic testing. *Nano Today* **9,** 166–171 (2014).
102. Agasti, S. S. *et al.* Nanoparticles for detection and diagnosis. *Advanced Drug Delivery Reviews* **62,** 316–328 (2010).
103. Gould, P. Nanoparticles probe biosystems. *Mater. Today* **7,** 36–43 (2004).
104. Brede, C. & Labhasetwar, V. Applications of Nanoparticles in the Detection andTreatment of Kidney Diseases. *Advances in Chronic Kidney Disease* **20,** 454–465 (2013).
105. Chinen, A. B. *et al.* Nanoparticle Probes for the Detection of Cancer Biomarkers, Cells, and Tissues by Fluorescence. *Chem. Rev.* **115,** 10530–10574 (2015).
106. Yeo, D., Wiraja, C., Chuah, Y. J., Gao, Y. & Xu, C. A Nanoparticle-based Sensor Platform for Cell Tracking and Status/Function Assessment. *Sci. Rep.* **5,** 14768 (2015).
107. Byrd, T. F. *et al.* The microfluidic multitrap nanophysiometer for hematologic cancer cell characterization reveals temporal sensitivity of the calcein-AM efflux assay. *Sci. Rep.* **4,** 5117 (2014).

108. Bratosin, D., Mitrofan, L., Palii, C., Estaquier, J. & Montreuil, J. Novel fluorescence assay using calcein-AM for the determination of human erythrocyte viability and aging. *Cytom. Part A* **66,** 78–84 (2005).
109. Jones, K. H. & Senft, J. A. An improved method to determine cell viability by simultaneous staining with fluorescein diacetate-propidium iodide. *J. Histochem. Cytochem.* **33,** 77–79 (1985).
110. Chen, S. J. & Chang, H. T. Nile red-adsorbed gold nanoparticles for selective determination of thiols based on energy transfer and aggregation. *Anal. Chem.* **76,** 3727–3734 (2004).
111. Ipe, B. I., Yoosaf, K. & Thomas, K. G. Functionalized gold nanoparticles as phosphorescent nanomaterials and sensors. *J. Am. Chem. Soc.* **128,** 1907–1913 (2006).
112. Medintz, I. L. *et al.* Proteolytic activity monitored by fluorescence resonance energy transfer through quantum-dot–peptide conjugates. *Nat. Mater.* **5,** 581–589 (2006).
113. Oh, E. *et al.* Inhibition Assay of Biomolecules based on Fluorescence Resonance Energy Transfer (FRET) between Quantum Dots and Gold Nanoparticles. *J. Am. Chem. Soc.* **127,** 3270–3271 (2005).
114. Park, J. I. W. *et al.* Nanoparticle-based energy transfer for rapid and simple detection of protein glycosylation. *Appl. Surf. Sci.* **45,** 1913–1920 (2008).
115. You, C.-C. *et al.* Detection and identification of proteins using nanoparticle–fluorescent polymer 'chemical nose' sensors. *Nat. Nanotechnol.* **2,** 318–323 (2007).
116. Dyadyusha, L. *et al.* Quenching of CdSe quantum dot emission, a new approach for biosensing. *Chem. Commun.* 3201 (2005). doi:10.1039/b500664c
117. Phillips, R. L., Miranda, O. R., You, C.-C., Rotello, V. M. & Bunz, U. H. F. Rapid and Efficient Identification of Bacteria Using Gold-Nanoparticle–Poly(para-phenyleneethynylene) Constructs. *Angew. Chemie Int. Ed.* **47,** 2590–2594 (2008).
118. Yang, L. & Li, Y. Simultaneous detection of Escherichia coli O157:H7 and Salmonella Typhimurium using quantum dots as fluorescence labels. *Analyst* **131,** 394–401 (2006).
119. Zhu, L., Ang, S. & Liu, W. T. Quantum Dots as a Novel Immunofluorescent Detection System for Cryptosporidium parvum and Giardia lamblia. *Appl. Environ. Microbiol.* **70,** 597–598 (2004).
120. Su, X. L. & Li, Y. Quantum dot biolabeling coupled with immunomagnetic separation for detection of Escherichia coli O1517:H7. *Anal. Chem.* **76,** 4806–4810 (2004).
121. Thomas, S. W., Joly, G. D. & Swager, T. M. Chemical sensors based on amplifying fluorescent conjugated polymers. *Chemical Reviews* **107,** 1339–1386 (2007).
122. Chalmers, N. I. *et al.* Use of quantum dot luminescent probes to achieve single-cell resolution of human oral bacteria in biofilms. *Appl. Environ. Microbiol.* **73,** 630–636 (2007).
123. Kloepfer, J. A. *et al.* Quantum dots as strain- and metabolism-specific microbiological labels. *Appl. Environ. Microbiol.* **69,** 4205–13 (2003).

124. Deisingh, A. K. & Thompson, M. Detection of infectious and toxigenic bacteria. *Analyst* **127,** 567–581 (2002).
125. Peng, X. H. *et al.* Targeted magnetic iron oxide nanoparticles for tumor imaging and therapy. *Int. J. Nanomedicine* **3,** 311–321 (2008).
126. Okassa, L. N. *et al.* Optimization of iron oxide nanoparticles encapsulation within poly(d,l-lactide-co-glycolide) sub-micron particles. *Eur. J. Pharm. Biopharm.* **67,** 31–38 (2007).
127. Reuveni, T., Motiei, M., Romman, Z., Popovtzer, A. & Popovtzer, R. Targeted gold nanoparticles enable molecular CT imaging of cancer: an in vivo study. *Int. J. Nanomedicine* **6,** 2859–2864 (2011).
128. Wolfbeis, O. S. An overview of nanoparticles commonly used in fluorescent bioimaging. *Chem. Soc. Rev.* **44,** 4743–4768 (2015).
129. Ueda, K. Glycoproteomic strategies: From discovery to clinical application of cancer carbohydrate biomarkers. *Proteomics - Clinical Applications* **7,** 607–617 (2013).
130. Füzéry, A. K., Levin, J., Chan, M. M. & Chan, D. W. Translation of proteomic biomarkers into FDA approved cancer diagnostics: issues and challenges. *Clin. Proteomics* **10,** 13 (2013).
131. Taton, T. A. Scanometric DNA Array Detection with Nanoparticle Probes. *Science (80-.).* **289,** 1757–1760 (2000).
132. Cao, Y. C., Jin, R. & Mirkin, C. A. Nanoparticles with Raman Spectroscopic Fingerprints for DNA and RNA Detection. *Science (80-.).* **297,** 1536–1540 (2002).
133. Xiang, D. *et al.* Nucleic acid aptamer-guided cancer therapeutics and diagnostics: The next generation of cancer medicine. *Theranostics* **5,** 23–42 (2015).
134. Hakomori, S. Tumor-associated carbohydrate antigens defining tumor malignancy: basis for development of anti-cancer vaccines. *Advances in experimental medicine and biology* **491,** 369–402 (2001).
135. Li, H., Cao, Z., Zhang, Y., Lau, C. & Lu, J. Simultaneous detection of two lung cancer biomarkers using dual-color fluorescence quantum dots. *Analyst* **136,** 1399 (2011).
136. Harding, M. *et al.* Neurone specific enolase (NSE) in small cell lung cancer: a tumour marker of prognostic significance? *Br. J. Cancer* **61,** 605–7 (1990).
137. Cao, Z., Li, H., Lau, C. & Zhang, Y. Cross-talk-free simultaneous fluoroimmunoassay of two biomarkers based on dual-color quantum dots. *Anal. Chim. Acta* **698,** 44–50 (2011).
138. Jokerst, J. V, Lobovkina, T., Zare, R. N. & Gambhir, S. S. Nanoparticle PEGylation for imaging and therapy. *Nanomedicine* **6,** 715–728 (2011).
139. Zhang, S., Li, J., Lykotrafitis, G., Bao, G. & Suresh, S. Size-dependent endocytosis of nanoparticles. *Adv. Mater.* **21,** 419–424 (2009).
140. Li-Shishido, S., Watanabe, T. M., Tada, H., Higuchi, H. & Ohuchi, N. Reduction in nonfluorescence state of quantum dots on an immunofluorescence staining. *Biochem. Biophys. Res. Commun.* **351,** 7–13 (2006).
141. Jin, Y., Ye, F., Zeigler, M., Wu, C. & Chiu, D. T. Near-infrared fluorescent dye-doped semiconducting polymer dots. *ACS Nano* **5,** 1468–1475 (2011).

142. Nune, S. K. *et al.* Nanoparticles for biomedical imaging. *Expert Opin. Drug Deliv.* **6,** (2009).
143. Wu, C., Bull, B., Szymanski, C., Christensen, K. & McNeill, J. Multicolor conjugated polymer dots for biological fluorescence imaging. *ACS Nano* **2,** 2415–2423 (2008).
144. Zhang, S., Gao, H. & Bao, G. Physical Principles of Nanoparticle Cellular Endocytosis. *ACS Nano* **9,** 8655–8671 (2015).
145. Yu, S.-B. & Watson, A. D. Metal-Based X-ray Contrast Media. *Chem. Rev.* **99,** 2353–2378 (1999).
146. Hainfeld, J. F., Slatkin, D. N., Focella, T. M. & Smilowitz, H. M. Gold nanoparticles: A new X-ray contrast agent. *Br. J. Radiol.* **79,** 248–253 (2006).
147. Kim, D., Park, S., Jae, H. L., Yong, Y. J. & Jon, S. Antibiofouling polymer-coated gold nanoparticles as a contrast agent for in vivo X-ray computed tomography imaging. *J. Am. Chem. Soc.* **129,** 7661–7665 (2007).
148. Hanini, A. *et al.* Evaluation of iron oxide nanoparticle biocompatibility. *Int. J. Nanomedicine* **6,** 787–794 (2011).
149. Hwu, J. R. *et al.* Targeted paclitaxel by conjugation to iron oxide and gold nanoparticles. *J. Am. Chem. Soc.* **131,** 66–68 (2009).
150. Jarrett, B. R., Frendo, M., Vogan, J. & Louie, A. Y. Size-controlled synthesis of dextran sulfate coated iron oxide nanoparticles for magnetic resonance imaging. *Nanotechnology* **18,** 35603 (2007).
151. Thorek, D. L. J. & Tsourkas, A. Size, charge and concentration dependent uptake of iron oxide particles by non-phagocytic cells. *Biomaterials* **29,** 3583–3590 (2008).
152. Gandon, Y. *et al.* [Super-paramagnetic iron oxide: an MRI contrast media for the reticuloendothelial system]. *Ann Radiol* **32,** 267–272 (1989).
153. Montet, X., Weissleder, R. & Josephson, L. Imaging Pancreatic Cancer with a Peptide - Nanoparticle Conjugate Targeted to Normal Pancreas. 905–911 (2006). doi:10.1021/BC060035+
154. Wunderbaldinger, P., Josephson, L., Bremer, C., Moore, A. & Weissleder, R. Detection of lymph node metastases by contrast-enhanced MRI in an experimental model. *Magn. Reson. Med.* **47,** 292–297 (2002).
155. Kircher, M. F. *et al.* In Vivo High Resolution Three-Dimensional Imaging of Antigen-Specific Cytotoxic T-Lymphocyte Trafficking to Tumors. *Cancer Res.* **63,** 6838–6846 (2003).
156. Kircher, M. F., Mahmood, U., King, R. S., Weissleder, R. & Josephson, L. A Multimodal Nanoparticle for Preoperative Magnetic Resonance Imaging and Intraoperative Optical Brain Tumor Delineation. *Cancer Res.* **63,** 8122–8125 (2003).
157. Lewin, M. *et al.* Tat peptide-derivatized magnetic nanoparticles allow in vivo tracking and recovery of progenitor cells. *Nat. Biotechnol.* **18,** 410–414 (2000).
158. Wunderbaldinger, P., Josephson, L. & Weissleder, R. Crosslinked iron oxides (CLIO): a new platform for the development of targeted MR contrast agents. *Acad Radiol* **9 Suppl 2,** S304-6 (2002).

159. Song, H. T. *et al.* Surface modulation of magnetic nanocrystals in the development of highly efficient magnetic resonance probes for intracellular labeling. *J. Am. Chem. Soc.* **127,** 9992–9993 (2005).
160. Miyoshi, S. *et al.* Transfection of neuroprogenitor cells with iron nanoparticles for magnetic resonance imaging tracking: Cell viability, differentiation, and intracellular localization. *Mol. Imaging Biol.* **7,** 286–295 (2006).
161. Soo Choi, H. *et al.* Renal clearance of quantum dots. *Nat. Biotechnol.* **25,** 1165–1170 (2007).
162. Smith, A. M., Duan, H., Mohs, A. M. & Nie, S. Bioconjugated quantum dots for in vivo molecular and cellular imaging. *Advanced Drug Delivery Reviews* **60,** 1226–1240 (2008).
163. Resch-Genger, U., Grabolle, M., Cavaliere-Jaricot, S., Nitschke, R. & Nann, T. Quantum dots versus organic dyes as fluorescent labels. *Nat. Methods* **5,** 763–775 (2008).
164. Gao, X., Cui, Y., Levenson, R. M., Chung, L. W. K. & Nie, S. In vivo cancer targeting and imaging with semiconductor quantum dots. *Nat. Biotechnol.* **22,** 969–976 (2004).
165. Cai, W. *et al.* Peptide-labeled near-infrared quantum dots for imaging tumor vasculature in living subjects. *Nano Lett.* **6,** 669–676 (2006).
166. Efros, A. L. & Nesbitt, D. J. Origin and control of blinking in quantum dots. *Nat. Nanotechnol.* **11,** 661–671 (2016).
167. Soenen, S. J. *et al.* The effect of nanoparticle degradation on poly(methacrylic acid)-coated quantum dot toxicity: The importance of particle functionality assessment in toxicology. *Acta Biomater.* **10,** 732–741 (2014).
168. Mancini, M. C., Kairdolf, B. A., Smith, A. M. & Nie, S. Oxidative quenching and degradation of polymer-encapsulated quantum dots: New insights into the long-term fate and toxicity of nanocrystals in vivo. *J. Am. Chem. Soc.* **130,** 10836–10837 (2008).
169. Houchin, M. L. & Topp, E. M. Physical properties of PLGA films during polymer degradation. *J. Appl. Polym. Sci.* **114,** 2848–2854 (2009).
170. Nuo Wang & Xue Shen Wu. Synthesis, characterization, biodegradation, and drug delivery application of biodegradable lactic/gly colic acid oligomers: Part II. Biodegradation and drug delivery application. *J. Biomater. Sci. Polym. Ed.* **9,** 75–87 (1998).
171. Uhrich, K. E., Cannizzaro, S. M., Langer, R. S. & Shakesheff, K. M. Polymeric Systems for Controlled Drug Release. *Chem. Rev.* **99,** 3181–3198 (1999).
172. Bartus, R. T., Tracy, M. A., Emerich, D. F. & Zale, S. E. Sustained delivery of proteins for novel therapeutic producs. *Science (80-.).* **281,** 1161–1162 (1998).
173. Ankrum, J. A. *et al.* Engineering cells with intracellular agent–loaded microparticles to control cell phenotype. *Nat. Protoc.* **9,** 233–245 (2014).
174. Cheng, J. *et al.* Formulation of functionalized PLGA-PEG nanoparticles for in vivo targeted drug delivery. *Biomaterials* **28,** 869–876 (2007).
175. Fu, X., Ping, Q. & Gao, Y. Effects of formulation factors on encapsulation efficiency and release behaviour in vitro of huperzine A-PLGA microspheres. *J. Microencapsul.* **22,** 705–714 (2005).

176. Xu, Y., Koo, D., Gerstein, E. & Kim, C.-S. Multi-scale modeling of polymer–drug interactions and their impact on the structural evolutions in PLGA-tetracycline films. *Polymer (Guildf).* **84,** 121–131 (2016).
177. Paliwal, R., Babu, R. J. & Palakurthi, S. Nanomedicine Scale-up Technologies: Feasibilities and Challenges. *AAPS PharmSciTech* **15,** 1527–1534 (2014).
178. McCall, R. L. & Sirianni, R. W. PLGA Nanoparticles Formed by Single- or Double-emulsion with Vitamin E-TPGS. *J. Vis. Exp.* **82,** (2013).
179. Feczkó, T., Tóth, J., Dósa, G. & Gyenis, J. Optimization of protein encapsulation in PLGA nanoparticles. *Chem. Eng. Process. Process Intensif.* **50,** 757–765 (2011).
180. Mahboubian, A., Hashemein, S. K., Moghadam, S., Atyabia, F. & Dinarvand, R. Preparation and in-vitro evaluation of controlled release PLGA microparticles containing triptoreline. *Iran. J. Pharm. Res.* **9,** 369–378 (2010).
181. Zhang, Y., Chan, H. F. & Leong, K. W. Advanced materials and processing for drug delivery: The past and the future. *Advanced Drug Delivery Reviews* **65,** 104–120 (2013).
182. Lawson, H. C. *et al.* Interstitial chemotherapy for malignant gliomas: The Johns Hopkins experience. *J. Neurooncol.* **83,** 61–70 (2007).
183. Bock, H. C. *et al.* First-line treatment of malignant glioma with carmustine implants followed by concomitant radiochemotherapy: A multicenter experience. *Neurosurg. Rev.* **33,** 441–449 (2010).
184. Liu, Z., Jiao, Y., Wang, Y., Zhou, C. & Zhang, Z. Polysaccharides-based nanoparticles as drug delivery systems. *Advanced Drug Delivery Reviews* **60,** 1650–1662 (2008).
185. Felt, O., Buri, P. & Gurny, R. Chitosan: A Unique Polysaccharide for Drug Delivery. *Drug Dev. Ind. Pharm.* **24,** 979–993 (1998).
186. Li, H., LaBean, T. H. & Leong, K. W. Nucleic acid-based nanoengineering: novel structures for biomedical applications. *Interface Focus* **1,** 702–724 (2011).
187. Andersen, E. S. *et al.* Self-assembly of a nanoscale DNA box with a controllable lid. *Nature* **459,** 73–76 (2009).
188. McNaughton, B. R., Cronican, J. J., Thompson, D. B. & Liu, D. R. Mammalian cell penetration, siRNA transfection, and DNA transfection by supercharged proteins. *Proc. Natl. Acad. Sci. U. S. A.* **106,** 6111–6116 (2009).
189. Cronican, J. J. *et al.* Potent delivery of functional proteins into mammalian cells in vitro and in vivo using a supercharged protein. *ACS Chem. Biol.* **5,** 747–752 (2010).
190. Hussain, M. A. *et al.* An efficient acetylation of dextran using in situ activated acetic anhydride with iodine. *J. Serbian Chem. Soc.* **75,** 165–173 (2010).
191. Bachelder, E. M., Pino, E. N. & Ainslie, K. M. Acetalated Dextran: A Tunable and Acid-Labile Biopolymer with Facile Synthesis and a Range of Applications. *Chemical Reviews* **117,** 1915–1926 (2017).
192. Bachelder, E. M. *et al.* In vitro analysis of acetalated dextran microparticles as a potent delivery platform for vaccine adjuvants. *Mol. Pharm.* **7,** 826–835 (2010).
193. Kauffman, K. J. *et al.* Synthesis and characterization of acetalated dextran polymer and microparticles with ethanol as a degradation product. *ACS Appl. Mater. Interfaces* **4,** 4149–4155 (2012).

194. Goldman, E. R. *et al.* A hybrid quantum dot - Antibody fragment fluorescence resonance energy transfer-based TNT sensor. *J. Am. Chem. Soc.* **127,** 6744–6751 (2005).
195. Sun, C., Lee, J. S. H. & Zhang, M. Magnetic nanoparticles in MR imaging and drug delivery. *Advanced Drug Delivery Reviews* **60,** 1252–1265 (2008).
196. Di Marco, M. *et al.* Colloidal stability of ultrasmall superparamagnetic iron oxide (USPIO) particles with different coatings. *Int. J. Pharm.* **331,** 197–203 (2007).
197. N.Fauconnier, J.N.Pons, J.Roger & A.Bee. Thiolation of Maghemite Nanoparticles by Dimercaptosuccinic Acid. *J. Colloid Interface Sci.* **194,** 427–433 (1997).
198. Schulze, E. *et al.* Cellular uptake and trafficking of a prototypical magnetic iron oxide label in vitro. *Investigative radiology* **30,** 604–610 (1995).
199. Park, J. Y., Daksha, P., Lee, G. H., Woo, S. & Chang, Y. Highly water-dispersible PEG surface modified ultra small superparamagnetic iron oxide nanoparticles useful for target-specific biomedical applications. *Nanotechnology* **19,** 365603 (2008).
200. Pandey, P. *et al.* Application of thiolated gold nanoparticles for the enhancement of glucose oxidase activity. *Langmuir* **23,** 3333–3337 (2007).
201. Wilson, R. The use of gold nanoparticles in diagnostics and detection. *Chem. Soc. Rev.* **37,** 2028 (2008).
202. Kattumuri, V. *et al.* Gum arabic as a phytochemical construct for the stabilization of gold nanoparticles: In vivo pharmacokinetics and X-ray-contrast-imaging studies. *Small* **3,** 333–341 (2007).
203. and, M.-C. D. & Astruc*, D. Gold Nanoparticles: Assembly, Supramolecular Chemistry, Quantum-Size-Related Properties, and Applications toward Biology, Catalysis, and Nanotechnology. (2003). doi:10.1021/CR030698+
204. Wangoo, N., Bhasin, K. K., Mehta, S. K. & Suri, C. R. Synthesis and capping of water-dispersed gold nanoparticles by an amino acid: Bioconjugation and binding studies. *J. Colloid Interface Sci.* **323,** 247–254 (2008).
205. Allen, T. M. & Cullis, P. R. Liposomal drug delivery systems: From concept to clinical applications. *Advanced Drug Delivery Reviews* **65,** 36–48 (2013).
206. Allen, T. M. & Cleland, L. G. Serum-induced leakage of liposome contents. *BBA - Biomembr.* **597,** 418–426 (1980).
207. Cabanes, A., Briggs, K. E., Gokhale, P. C., Treat, J. A. & Rahman, A. Comparative in vivo studies with paclitaxel and liposome-encapsulated paclitaxel. *Int. J. Oncol.* **12,** 1035–1040 (1998).
208. Allen, T. M. A study of phospholipid interactions between high-density lipoproteins and small unilamellar vesicles. *BBA - Biomembr.* **640,** 385–397 (1981).
209. P.R.Cullis & M.J.Hope. The bilayer stabilizing role of sphingomyelin in the presence of cholesterol. A 31P NMR study. *Biochim. Biophys. Acta - Biomembr.* **597,** 533–542 (1980).
210. R.Cullis, P. Lateral diffusion rates of phosphatidylcholine in vesicle membranes: Eeffects of cholesterol and hydrocarbon phase transitions. *FEBS Lett.* **70,** 223–228 (1976).
211. J.McIntosh, T. The effect of cholesterol on the structure of phosphatidylcholine bilayers. *Biochim. Biophys. Acta - Biomembr.* **513,** 43–58 (1978).

212. D.Mayer, L. *et al.* Characterization of liposomal systems containing doxorubicin entrapped in response to pH gradients. *Biochim. Biophys. Acta - Biomembr.* **1025,** 143–151 (1990).
213. Haran, G., Cohen, R., Bar, L. K. & Barenholz, Y. Transmembrane ammonium sulfate gradients in liposomes produce efficient and stable entrapment of amphipathic weak bases. *BBA - Biomembr.* **1151,** 201–215 (1993).
214. Yameen, B. *et al.* Insight into nanoparticle cellular uptake and intracellular targeting. *J. Control. Release* **190,** 485–499 (2014).
215. Braet, F. *et al.* Contribution of high-resolution correlative imaging techniques in the study of the liver sieve in three-dimensions. *Microscopy Research and Technique* **70,** 230–242 (2007).
216. Blanco, E., Shen, H. & Ferrari, M. Principles of nanoparticle design for overcoming biological barriers to drug delivery. *Nat. Biotechnol.* **33,** 941–951 (2015).
217. Perrault, S. D., Walkey, C., Jennings, T., Fischer, H. C. & Chan, W. C. W. Mediating tumor targeting efficiency of nanoparticles through design. *Nano Lett.* **9,** 1909–1915 (2009).
218. Jain, R. K. & Stylianopoulos, T. Delivering nanomedicine to solid tumors. *Nat. Rev. Clin. Oncol.* **7,** 653–664 (2010).
219. Lee, H., Fonge, H., Hoang, B., Reilly, R. M. & Allen, C. The effects of particle size and molecular targeting on the intratumoral and subcellular distribution of polymeric nanoparticles. *Mol. Pharm.* **7,** 1195–1208 (2010).
220. Jiang, W., Kim, B. Y. S., Rutka, J. T. & Chan, W. C. W. Nanoparticle-mediated cellular response is size-dependent. *Nat. Nanotechnol.* **3,** 145–150 (2008).
221. Yuan, H., Li, J., Bao, G. & Zhang, S. Variable nanoparticle-cell adhesion strength regulates cellular uptake. *Phys. Rev. Lett.* **105,** 138101 (2010).
222. Paliwal, R., Babu, R. J. & Palakurthi, S. Nanomedicine Scale-up Technologies: Feasibilities and Challenges. *AAPS PharmSciTech* **15,** 1527–1534 (2014).
223. Hock, S. C., Ying, Y. M. & Wah, C. L. A review of the current scientific and regulatory status of nanomedicines and the challenges ahead. *PDA J. Pharm. Sci. Technol.* **65,** 177–95 (2011).
224. Liu, L., Bagia, C. & Janjic, J. M. The First Scale-Up Production of Theranostic Nanoemulsions. *Biores. Open Access* **4,** 218–28 (2015).
225. Fröhlich, E. The role of surface charge in cellular uptake and cytotoxicity of medical nanoparticles. *International Journal of Nanomedicine* **7,** 5577–5591 (2012).
226. Sahdev, P., Ochyl, L. J. & Moon, J. J. Biomaterials for nanoparticle vaccine delivery systems. *Pharm. Res.* **31,** 2563–2582 (2014).
227. Qiu, Y. *et al.* Surface chemistry and aspect ratio mediated cellular uptake of Au nanorods. *Biomaterials* **31,** 7606–7619 (2010).
228. Li, H. & Qian, Z. M. Transferrin/transferrin receptor-mediated drug delivery. *Medicinal Research Reviews* **22,** 225–250 (2002).
229. Huang, L. & Guo, S. Nanoparticles escaping RES and endosome: Challenges for siRNA delivery for cancer therapy. *Journal of Nanomaterials* **2011,** 1–12 (2011).
230. Geng, Y. *et al.* Shape effects of filaments versus spherical particles in flow and drug delivery. *Nat. Nanotechnol.* **2,** 249–255 (2007).

231. Chithrani, B. D., Ghazani, A. A. & Chan, W. C. W. Determining the size and shape dependence of gold nanoparticle uptake into mammalian cells. *Nano Lett.* **6,** 662–668 (2006).
232. Gratton, S. E. A. *et al.* The effect of particle design on cellular internalization pathways. *Proc. Natl. Acad. Sci.* **105,** 11613–11618 (2008).
233. ThermoFisher & Scientific. Carbodiimide Crosslinker Chemistry. (2016). Available at: https://www.thermofisher.com/us/en/home/life-science/protein-biology/protein-biology-learning-center/protein-biology-resource-library/pierce-protein-methods/carbodiimide-crosslinker-chemistry.html. (Accessed: 16th October 2017)
234. Scientific, T. F. Avidin-biotin interaction. Available at: https://www.thermofisher.com/us/en/home/life-science/protein-biology/protein-biology-learning-center/protein-biology-resource-library/pierce-protein-methods/avidin-biotin-interaction.html. (Accessed: 16th October 2017)
235. Torchilin, V. P. Recent advances with liposomes as pharmaceutical carriers. *Nat. Rev. Drug Discov.* **4,** 145–160 (2005).
236. Jahn, A. *et al.* Preparation of nanoparticles by continuous-flow microfluidics. *Journal of Nanoparticle Research* **10,** 925–934 (2008).
237. Valencia, P. M., Farokhzad, O. C., Karnik, R. & Langer, R. Microfluidic technologies for accelerating the clinical translation of nanoparticles. *Nat. Nanotechnol.* **7,** 623–629 (2012).
238. Li, H. Y. & Zhang, F. Preparation of nanoparticles by spray-drying and their use for efficient pulmonary drug delivery. *Methods Mol. Biol.* **906,** 295–301 (2012).
239. Lee, S. H., Heng, D., Ng, W. K., Chan, H. K. & Tan, R. B. H. Nano spray drying: A novel method for preparing protein nanoparticles for protein therapy. *Int. J. Pharm.* **403,** 192–200 (2011).
240. Jaworek, A. Micro- and nanoparticle production by electrospraying. *Powder Technology* **176,** 18–35 (2007).
241. Bilati, U., Allémann, E. & Doelker, E. Development of a nanoprecipitation method intended for the entrapment of hydrophilic drugs into nanoparticles. *Eur. J. Pharm. Sci.* **24,** 67–75 (2005).
242. Govender, T., Stolnik, S., Garnett, M. C., Illum, L. & Davis, S. S. PLGA nanoparticles prepared by nanoprecipitation: Drug loading and release studies of a water soluble drug. *J. Control. Release* **57,** 171–185 (1999).
243. Heath, J. R., Ribas, A. & Mischel, P. S. Single-cell analysis tools for drug discovery and development. *Nat. Rev. Drug Discov.* **15,** 204–216 (2015).
244. Shi, Q. *et al.* Single-cell proteomic chip for profiling intracellular signaling pathways in single tumor cells. *Proc. Natl. Acad. Sci.* **109,** 419–424 (2012).
245. Patel, A. P. *et al.* Single-cell RNA-seq highlights intratumoral heterogeneity in primary glioblastoma. *Science (80-.).* **321,** 1095–100 (2008).
246. Luo, Y. *et al.* Single-cell transcriptome analyses reveal signals to activate dormant neural stem cells. *Cell* **161,** 1175–1188 (2015).
247. Tang, F. *et al.* mRNA-Seq whole-transcriptome analysis of a single cell. *Nat. Methods* **6,** 377–382 (2009).
248. Hughes, A. J. *et al.* Single-cell western blotting. *Nat. Methods* **11,** 749–55 (2014).

249. Kress, W. J. & Erickson, D. L. DNA barcodes: Genes, genomics, and bioinformatics. *Proc. Natl. Acad. Sci.* **105,** 2761–2762 (2008).
250. Castellarnau, M., Szeto, G. L., Irvine, D. J., Love, J. C. & Voldman, J. Stochastic barcoding for single-cell tracking. in *17th International Conference on Miniaturized Systems for Chemistry and Life Sciences, MicroTAS 2013* **1,** 690–692 (2013).
251. Rees, P. *et al.* Nanoparticle vesicle encoding for imaging and tracking cell populations. *Nat. Methods* **11,** 1177–1181 (2014).
252. Pollen, A. A. *et al.* Low-coverage single-cell mRNA sequencing reveals cellular heterogeneity and activated signaling pathways in developing cerebral cortex. *Nat. Biotechnol.* **32,** 1053–1058 (2014).
253. Lu, Y. *et al.* Highly multiplexed profiling of single-cell effector functions reveals deep functional heterogeneity in response to pathogenic ligands. *Proc. Natl. Acad. Sci.* **112,** E607–E615 (2015).
254. Tritschler, S., Theis, F. J., Lickert, H. & Böttcher, A. Systematic single-cell analysis provides new insights into heterogeneity and plasticity of the pancreas. *Molecular Metabolism* **6,** 974–990 (2017).
255. Ward-hartstonge, K. A. & Kemp, R. A. Regulatory T-cell heterogeneity and the cancer immune response. *Nat. Publ. Gr.* **6,** e154 (2017).
256. Invitrogen. Propidium Iodide Nucleic Acid Stain. *Molecular Probes - Invitrogen detection technologies* 1–5 (2006). doi:10.1101/pdb.caut676
257. Polchert, D. *et al.* IFN-gamma activation of mesenchymal stem cells for treatment and prevention of graft versus host disease. *Eur. J. Immunol.* **38,** 1745–55 (2008).
258. Arnspang Christensen, E., Kulatunga, P. & Lagerholm, B. C. A Single Molecule Investigation of the Photostability of Quantum Dots. *PLoS One* **7,** (2012).
259. Shi, X., Tu, Y., Liu, X., Yeung, E. S. & Gai, H. Photobleaching of quantum dots by non-resonant light. *Phys. Chem. Chem. Phys.* **15,** 3130 (2013).
260. Dayal, S. & Burda, C. Surface effects on quantum dot-based energy transfer. *J. Am. Chem. Soc.* **129,** 7977–7981 (2007).
261. Chashchikhin, O. V. & Budyka, M. F. Photoactivation, photobleaching and photoetching of CdS quantum dots − Role of oxygen and solvent. *J. Photochem. Photobiol. A Chem.* **343,** 72–76 (2017).
262. Yu, J., Rong, Y., Kuo, C.-T., Zhou, X.-H. & Chiu, D. T. Recent Advances in the Development of Highly Luminescent Semiconducting Polymer Dots and Nanoparticles for Biological Imaging and Medicine. *Anal. Chem.* **89,** 42–56 (2017).
263. Wu, C. & Chiu, D. T. Highly fluorescent semiconducting polymer dots for biology and medicine. *Angewandte Chemie - International Edition* **52,** 3086–3109 (2013).
264. Li, Y. *et al.* Polymer Dots for Photoelectrochemical Bioanalysis. *Anal. Chem.* **89,** 4945–4950 (2017).
265. Ogden, C. L., Carroll, M. D., Fryar, C. D. & Flegal, K. M. *Prevalence of Obesity Among Adults and Youth: United States, 2011–2014*. (2015).
266. Ogden, C. L., Carroll, M. D., Kit, B. K. & Flegal, K. M. Prevalence of Childhood and Adult Obesity in the United States, 2011-2012. *JAMA* **311,** 806 (2014).
267. Cynthia L. Ogden, Molly M. Lamb;, Margaret D. Carroll & Katherine M. Flegal. *Obesity and Socioeconomic Status in Adults: United States, 2005–2008*. (2010).

268. Grundlingh, J., Dargan, P. I., El-Zanfaly, M. & Wood, D. M. 2,4-Dinitrophenol (DNP): A Weight Loss Agent with Significant Acute Toxicity and Risk of Death. *Journal of Medical Toxicology* **7,** 205–212 (2011).
269. Jastroch, M., Keipert, S. & Perocchi, F. From explosives to physiological combustion: Next generation chemical uncouplers. *Molecular Metabolism* **3,** 86–87 (2014).
270. Kenwood, B. M. *et al.* Identification of a novel mitochondrial uncoupler that does not depolarize the plasma membrane. *Mol. Metab.* **3,** 114–123 (2014).
271. Berbée, J. F. P. *et al.* Brown fat activation reduces hypercholesterolaemia and protects from atherosclerosis development. *Nat. Commun.* **6,** 6356 (2015).
272. Siegfried Ussar1, 2, Kevin Y. Lee1, Simon N. Dankel1, 3, 4, Jeremie Boucher1, M.-F., Haering1, Andre Kleinridders1, Thomas Thomou1, Ruidan Xue1, Yazmin Macotela1,†, A. & M. Cypess1, Yu-Hua Tseng1, Gunnar Mellgren3, 4, and C. R. K. Asc-1, PAT2 and P2RX5 are novel cell surface markers for white, beige and brown adipocytes. *Sci Transl Med.* **27,** 286–296 (2015).
273. Azhdarinia, A. *et al.* A peptide probe for targeted brown adipose tissue imaging. *Nat. Commun.* **4,** 1–11 (2013).
274. van Dam, A. D., Boon, M. R., Berb??e, J. F. P., Rensen, P. C. N. & van Harmelen, V. Targeting white, brown and perivascular adipose tissue in atherosclerosis development. *Eur. J. Pharmacol.* 1–11 (2016). doi:10.1016/j.ejphar.2017.03.051
275. Camastra, S. *et al.* Muscle and adipose tissue morphology, insulin sensitivity and beta-cell function in diabetic and nondiabetic obese patients: effects of bariatric surgery. *Sci. Rep.* **7,** 9007 (2017).
276. Boutens, L. & Stienstra, R. Adipose tissue macrophages: going off track during obesity. *Diabetologia* **59,** 879–894 (2016).